

Regulation of Photosynthesis in Bloom-Forming Cyanobacteria with the Simplest β -Diketone

Mihebai Yilimulati,[○] Jiyuan Jin,[○] Xin Wang,[○] Xiaomeng Wang, Dmitry Shevela, Bing Wu, Kai Wang, Lang Zhou, Yunlu Jia, Bingcai Pan, Govindjee Govindjee, and Shujuan Zhang*



Cite This: <https://doi.org/10.1021/acs.est.1c04683>



Read Online

ACCESS |



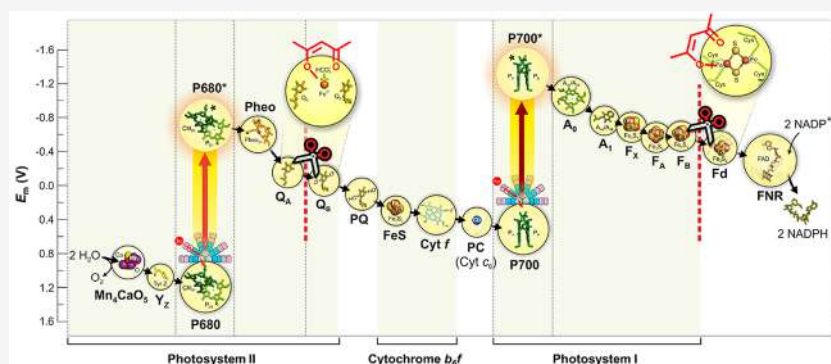
Metrics & More



Article Recommendations



Supporting Information



ABSTRACT: Selective inhibition of photosynthesis is a fundamental strategy to solve the global challenge caused by harmful cyanobacterial blooms. However, there is a lack of specificity of the currently used cyanocides, because most of them act on cyanobacteria by generating nontargeted oxidative stress. Here, for the first time, we find that the simplest β -diketone, acetylacetone, is a promising specific cyanocide, which acts on *Microcystis aeruginosa* through targeted binding on bound iron species in the photosynthetic electron transport chain, rather than by oxidizing the components of the photosynthetic apparatus. The targeted binding approach outperforms the general oxidation mechanism in terms of specificity and eco-safety. Given the essential role of photosynthesis in both natural and artificial systems, this finding not only provides a unique solution for the selective control of cyanobacteria but also sheds new light on the ways to modulate photosynthesis.

KEYWORDS: Acetylacetone, *Microcystis aeruginosa*, Algicide, Cyanocide, Harmful Algal Bloom

INTRODUCTION

Photosynthesis is the most important global chemical process, which maintains life on Earth by providing oxygen, food, and fuel for our survival.^{1,2} Cyanobacteria, the only oxygen-evolving prokaryotes that obtain energy through photosynthesis, are fundamentally important in our biosphere because of their role in the supply of oxygen, sequestration of carbon dioxide, and nitrogen fixation.^{3,4} However, due to the global climate change and eutrophication, some bloom-forming cyanobacteria proliferate under suitable environmental conditions to a high biomass and produce extremely dangerous toxins, resulting in harmful cyanobacterial and/or algal blooms (HABs).^{5–8} HABs create dead zones in water bodies and lead to huge economic loss; freshwater HABs in the USA alone result in an annual economic loss of more than 4 billion US dollars.⁷ The overall situation has been exacerbated over the last four decades.^{7,8}

Although great efforts have been, and are being, made to deal with HABs, their control remains a big challenge.^{5,9} A fundamental solution for bloom control is to restrict nutrient

inputs to mitigate eutrophication. However, this solution will take many years to become effective and is currently impractical for most of the areas across the world due to economic reasons.^{10,11} In recent decades, much attention has been paid to strategies that are based on general algicidal approaches, especially for the urgent treatment of bloom outbreaks.¹¹ All of the cyanocides used thus far have been derived from either pesticides (herbicides, fungicides, insecticides) or disinfectants (Figure 1). The generation of oxidative stress is the fundamental action mechanism of these disinfectants. Since oxidative stress is not target-selective, the utilization of disinfectants, such as hydrogen peroxide (H_2O_2) and permanganate, constitutes a threat to biodiversity. Efforts

Received: July 15, 2021

Revised: August 30, 2021

Accepted: September 13, 2021

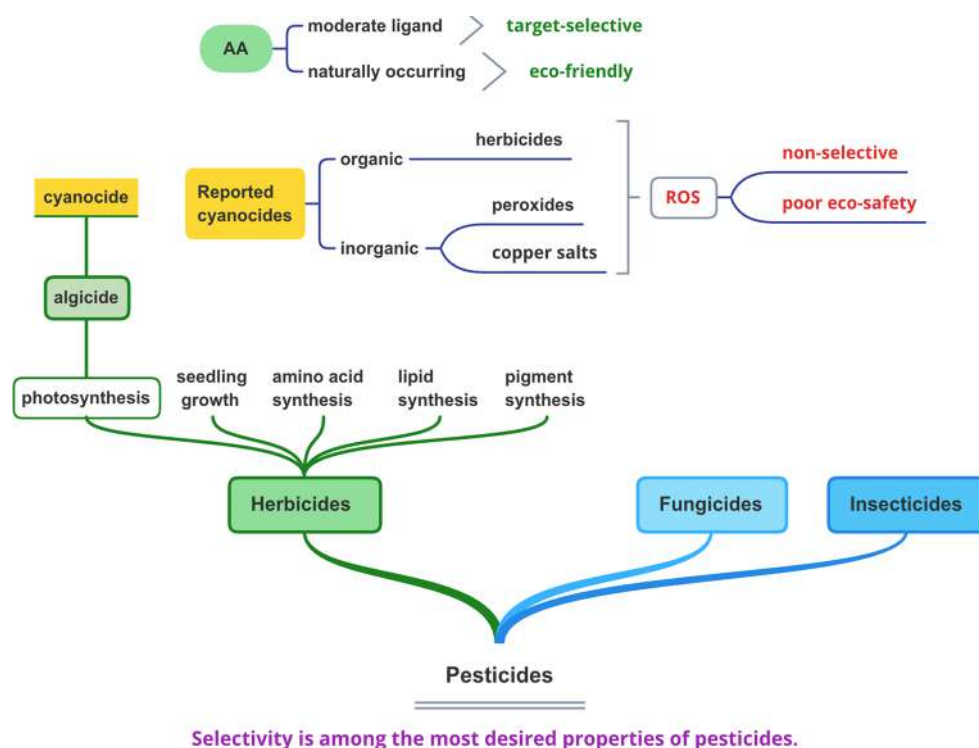


Figure 1. Development history and the most desired properties of cyanocides. ROS: reactive oxygen species. See ref 12 for further details on the action mechanisms of the pesticides.

toward the chemical control of HABs have been made on the screening of suitable herbicides, since one of the outstanding action mechanisms of herbicides is the inhibition of photosynthesis.¹² However, most of the herbicides are not specific to cyanobacteria, and the unwanted accumulation of herbicides in the environment is still a major concern around the world.¹² In order to minimize eco-risks, allelochemicals, produced by plants, algae, bacteria, and fungi, have been investigated as cyanocides.¹³ Nevertheless, the use of allelochemicals is still limited because of low effectiveness or poor economic efficiency.¹³ When eco-safety and sustainability are taken into account, chemicals that function as specific cyanocides need to be fully explored and exploited.

Cyanobacteria, unlike algae and other higher plants, do not have chloroplasts *per se*. The photosynthetic apparatus of cyanobacteria is much less protected, providing us the possibility of regulating it in subtle ways. Here, we show that the simplest β -diketone, acetylacetone (AA), which is naturally present in fruits and vegetables and known to function as a photoinduced electron shuttle,¹⁴ is a specific cyanocide for the freshwater cyanobacteria *Microcystis aeruginosa*. Unlike all other known cyanocides, AA acts on *Microcystis aeruginosa* in a nonoxidative way: it selectively interferes with the photosynthetic electron transport chain by binding to the nonheme iron in Photosystem II (PSII) and the iron–sulfur clusters in ferredoxin. To the best of our knowledge, this is the first report on the inhibition of cyanobacteria through a nonoxidative and metal-binding pathway. This finding provides a clear and definite potential for the control of cyanobacterial blooms in an eco-sustainable way.

EXPERIMENTAL SECTION

Chemicals and Materials. Acetylacetone (AA, 99%), was purchased from Aladdin Industrial Corporation (Shanghai,

China). Hydrogen peroxide (H_2O_2 , 30 wt %) was obtained from Sinopharm Chemical Reagent Co., Ltd. (Shanghai, China). Microcystin-leucine-arginine (MC-LR, 95%) was purchased from Taiwan Algal Science Inc. Other chemicals used in analysis are presented in Text S1.

Culturing *Microcystis aeruginosa* and *Lemna minor*.

Cells of *Microcystis aeruginosa* were incubated at 25 °C in a sterile BG-11 medium under 40 $\mu\text{mol photons m}^{-2} \text{s}^{-1}$ of constant cool-fluorescent light (light/dark cycle, 12 h/12 h) in an incubation cabinet. *Lemna minor* was cultivated in raw pond water under conditions otherwise identical with those used for *Microcystis aeruginosa*. More details on culturing and sampling of *Microcystis aeruginosa* and *Lemna minor* are presented in Text S2.

Inhibition Experiments. The culture solution of *Microcystis aeruginosa* was diluted to an OD_{680} (the optical density at a wavelength of 680 nm) value of about 0.2 (corresponding to a cell density of $5 \times 10^6 \text{ cells mL}^{-1}$) with the sterile BG11 medium. Aliquots of 100 mL of the diluted cell suspensions were employed for inhibition experiments by adding cyanocides to the desired concentrations (0.02–0.1 mM for AA and H_2O_2 , 0.1 mM for AA- $(\text{CH}_3)_2$, AA-Cl, and diacetyl). Solutions without the addition of any cyanocide were the blank controls. Each type of sample was run in three replicates. A 5 mL aliquot of the suspension was sampled during the incubation to monitor the growth status. All sampling operations were carried out in a sterile, ultraclean cabinet.

Analysis of Cell Structure, Membrane Integrity, and Cell Viability. The ultrastructure of the cells was observed with a transmission electron microscope (JEM1200EX, JEOL, Japan). The integrity of cells was determined using SYTOX green nucleic acid stain (Thermo Fisher, USA). The viability of the cells was determined with the Annexin V-FITC apoptosis detection kit (see Text S3 for more details).

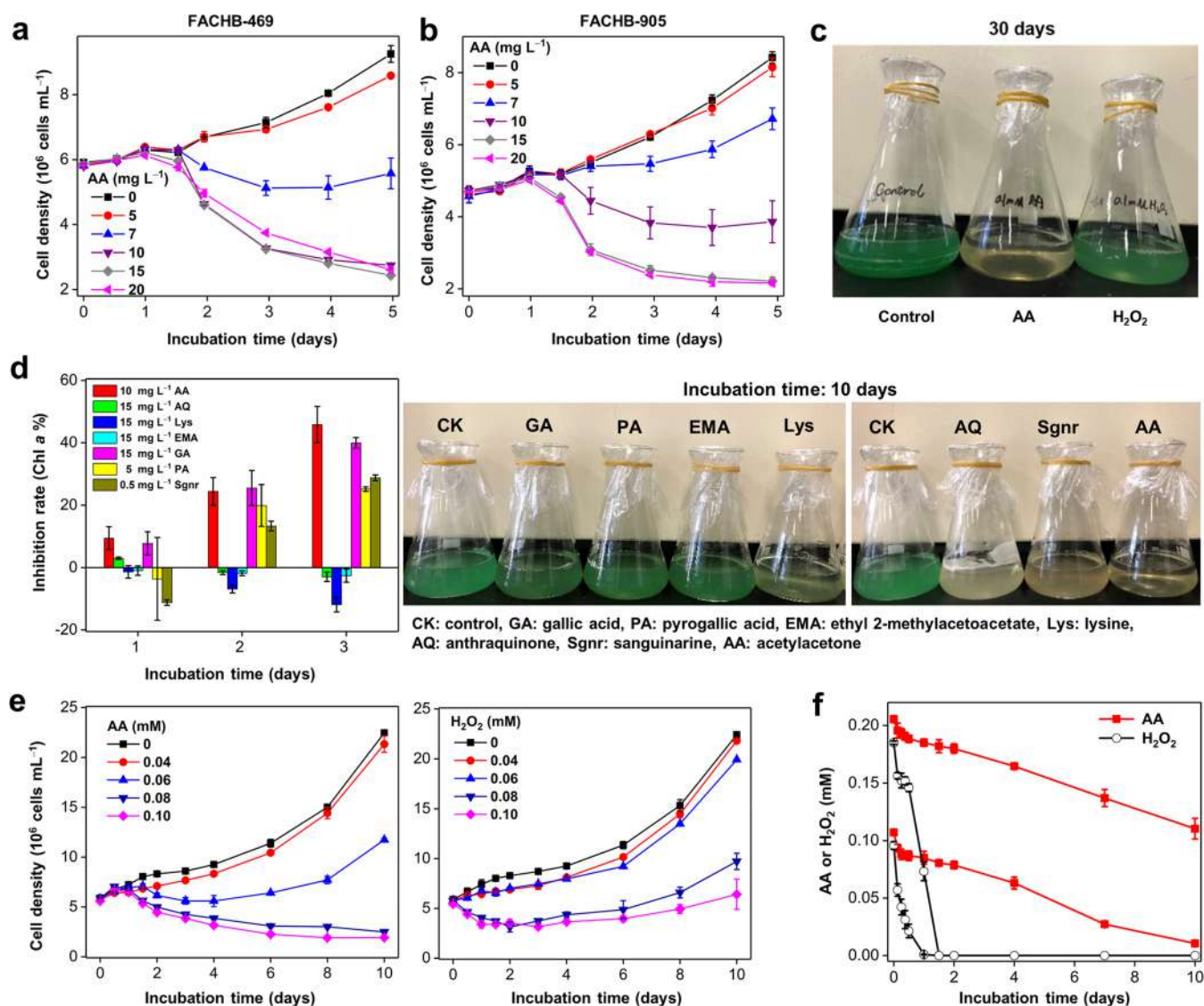


Figure 2. Cyanocidal performance comparison of acetylacetone (AA) with several other commonly used cyanocides on *Microcystis*. (a, b) Inhibition effects of AA on the growth of toxic strain FACHB-905 and nontoxic strain FACHB-469, respectively. (c) Photograph of FACHB-905 cultures after 30 days of incubation with 0.1 mM of AA and H_2O_2 . (d) Comparison of AA with several natural compounds (the symbols are defined below the right picture) on FACHB-905: (left) inhibition of Chl *a*; (right) photograph of the cultures after 10 days of incubation. (e) Inhibition of cell growth (FACHB-905) by AA and H_2O_2 at different concentrations. (f) Time dependence of the depletion of AA and H_2O_2 in the incubated FACHB-905 cultures.

Analysis of Cyanocides, Photosynthetic Pigments, Enzymes, and Metabolites. The concentrations of AA and MC-LR were determined by a chromatographic method. The concentration of H_2O_2 was measured by the *N,N*-diethyl-*p*-phenylenediamine/peroxidase (DPD/POD) method. The photosynthetic pigments were quantified with a UV–vis spectrophotometer (UV-2700, Shimadzu Co., Japan). Commercial assay kits for reactive oxygen species (ROS), malondialdehyde (MDA), superoxide dismutase (SOD), peroxidase (POD), and reduced glutathione (GSH) (Nanjing Jiancheng, China) were used to determine the activities of antioxidant enzymes. Excitation–emission fluorescence spectra of metabolites were recorded with a fluorescence spectrophotometer. More details are available in Text S4.

Monitoring of the Physiological Status of *Microcystis aeruginosa*. Photosynthetic activities were determined with a PHYTO-PAM phytoplankton analyzer (Walz, Germany), which provides both the effective quantum yield (Φ_e) and

the electron transport rate (ETR) of PSII. Further, a plant efficiency analyzer (Handy PEA, Hansatech, UK) was used to measure the Chlorophyll (Chl) *a* fluorescence transient, from which the JIP test was made; in addition, a liquid-phase oxygen electrode system (Oxytherm+R, Hansatech, U.K.) was used to monitor the rates of oxygen evolution. More details of these experiments are presented in Text S5.

Omics Assay. The metabolites were analyzed with a gas chromatography–mass spectrometry (GC-MS) system (Agilent 7890B-5977B, USA). The data set of the relative abundance of metabolites was processed for multivariate analysis. Proteins were analyzed with a liquid chromatography–tandem mass spectrometer (LC-MS/MS) (Q Exactive Plus, Thermo Fisher, USA). Gene ontology (GO) annotations (<http://geneontology.org/>) and Kyoto Encyclopedia of Genes and Genomes (KEGG) annotations (<http://www.kegg.jp/kegg/mapper.html>) were used to analyze proteins (see Text S6 for more details).

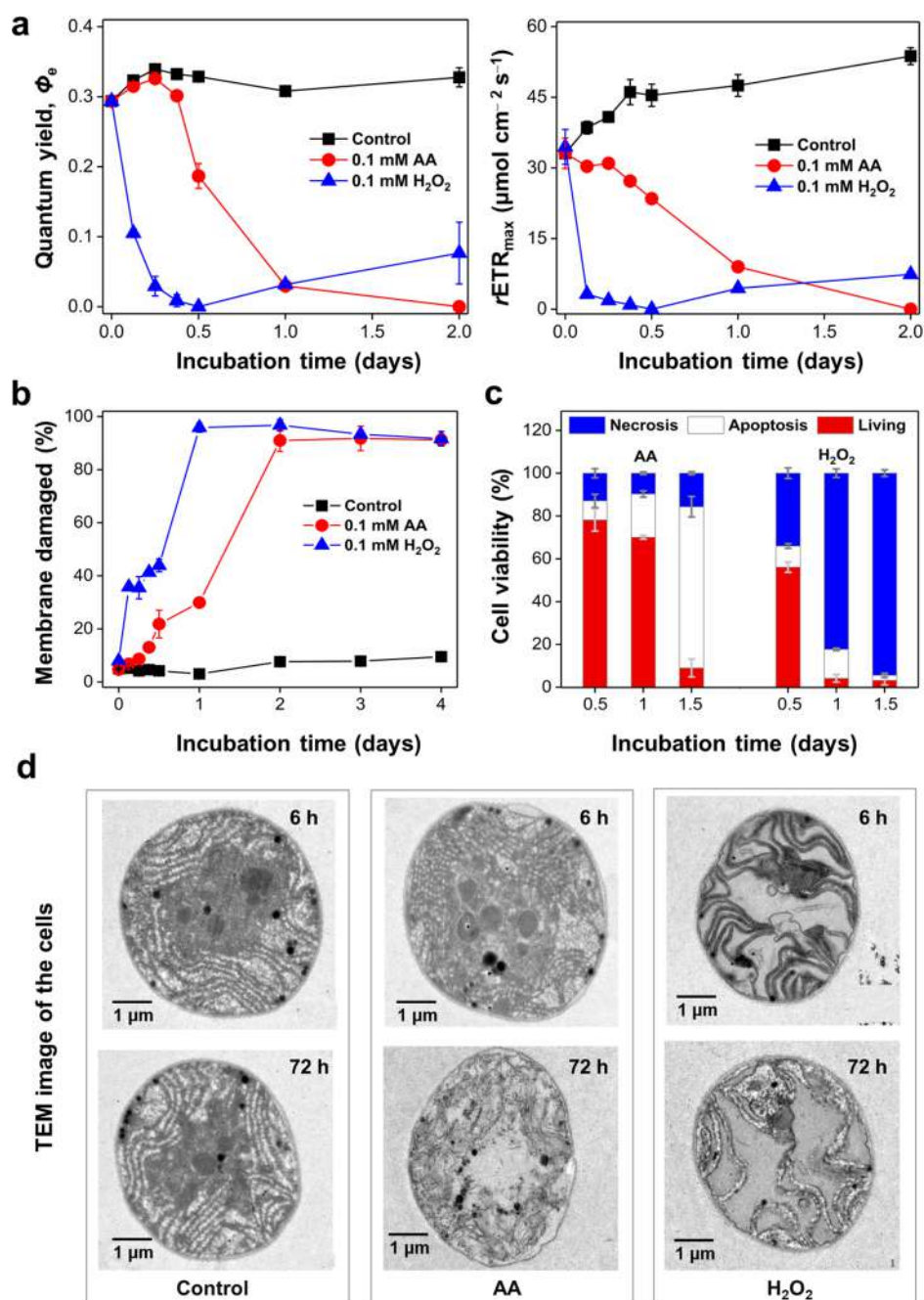


Figure 3. Physiological changes in AA- and H_2O_2 -treated FACHB-905 cells. (a) Photosynthetic performance in terms of the effective quantum yield (Φ_e) and the maximum relative electron transport rate ($rETR_{max}$). (b) Membrane damage caused by AA and H_2O_2 . (c) Cell viability in AA- and H_2O_2 -incubated cultures. (d) Transmission electron microscopy (TEM) images of AA- and H_2O_2 -treated cells. Concentration of AA and H_2O_2 : 0.1 mM.

Statistical Analysis. All experiments were conducted in triplicate. Data are reported as the mean \pm standard deviation. One-way and two-way analysis of variance (ANOVA) were conducted for statistical analysis. t tests were performed to evaluate significant differences in our data.

RESULTS AND DISCUSSION

Effectiveness of AA on *Microcystis aeruginosa*. Oxidative stress is one of the main causes for the inactivation of many organisms, including cyanobacteria.^{15,16} *Microcystis* is a dominant bloom-forming species of cyanobacteria, which is known to generate extremely toxic microcystin. Microcystin

plays a protective role in *Microcystis* against oxidative stress and is therefore beneficial to this organism in keeping its population high.^{17,18} Here, we have found that AA is effective not only in the nontoxic *Microcystis aeruginosa* strain FACHB-469 (Figure 2a) but also in the toxic strain FACHB-905 (Figure 2b). Unless otherwise stated, we have used the toxic strain FACHB-905 in this work. For this strain, the 96 h ErC_{50} (i.e., the effective concentration of a substance causing 50% of the maximum response in terms of reduction of growth rate) value of AA was 7 mg L^{-1} (Figure 2b), which was much lower than those for *Chlorococcales* (green algae) (96 h ErC_{50} : 300 mg L^{-1}), fishes (96 h LC_{50} : 60–175 mg L^{-1}), shrimps (96 h

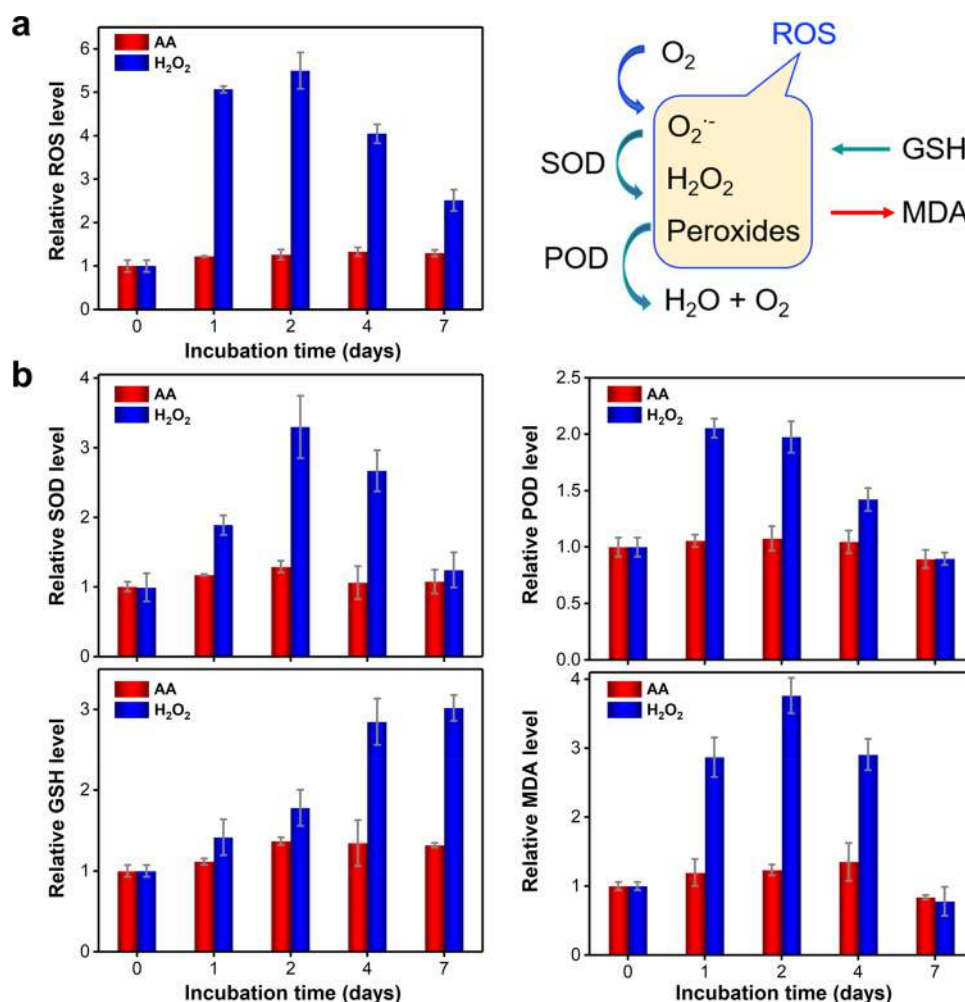


Figure 4. Oxidative stress analysis of AA- and H₂O₂-incubated FACHB-905 cells. (a) ROS levels in AA- and H₂O₂-incubated cells (left) and the reactions of ROS in cells (right). (b) Contents of antioxidative enzymes (SOD, POD, GSH) and the lipid oxidation product (MDA) in incubated cells of FACHB-905. All were determined with assay kits. Abbreviations: ROS, reactive oxygen species; SOD, superoxide dismutase; POD, peroxidase; GSH, glutathione; MDA, malondialdehyde. The concentration levels were expressed as relative values with the control as the reference.

EC₅₀: 217–631 mg L⁻¹), and *Daphnia magna* (48 h EC₅₀: 35–75 mg L⁻¹) (Table S1). These data demonstrate that AA has a very high selective toxicity for *Microcystis*.

The growth of *Microcystis aeruginosa* involves the exponential phase (0–25 days), the stationary phase (25–35 days), and the declining phase (35–45 days).¹⁹ One-time treatment with 10 mg L⁻¹ (equivalent to 0.1 mM) of AA was shown to inhibit the growth of FACHB-905 for more than 30 days (Figure 2c). During this period, the growth of *Microcystis aeruginosa* changed from the stationary phase to the declining phase, which significantly reduced the possibility for its rebloom.

Performance Comparison with Other Cyanocides. A series of natural compounds (allelochemicals), such as gallic acid, pyrogallol, anthraquinone, lysine, ethyl 2-methylacetoacetate, and sanguinarine, have been proposed to act as potential cyanocides.^{5,9–11} Our results clearly show that AA works better than most of these allelochemicals (Figure 2d). More importantly, AA has better biocompatibility with many other living systems in the environment (Text S7 and Table S1) and is much cheaper to use (Table S2).

In recent years, H₂O₂ has been reported to be a general as well as a selective algicide, depending on its concentration.²⁰

Addition of 2–10 mg L⁻¹ H₂O₂ can suppress cyanobacterial blooms, while eukaryotic algae, such as diatoms and green algae, are much less affected.²⁰ The selection of H₂O₂ as a cyanocide has been based on the following observations. (1) Cyanobacteria and eukaryotic algae have differences in sensitivity to oxidative stress; chloroplasts of eukaryotic organisms produce H₂O₂ in the Mehler reaction, while cyanobacteria produce water directly without H₂O₂ formation.¹⁵ Thus, cyanobacteria have a lower defense mechanism against H₂O₂ in comparison to eukaryotic phytoplankton species.¹⁵ (2) H₂O₂ is present in sunlight-exposed water because of its physiologically mediated synthesis as well as its generation through photolysis of organic matter.²¹ Under the conditions in this work, the ErC₅₀ value of H₂O₂ (2 mg L⁻¹) was lower than that of AA (Figure 2e). Moreover, the duration of the H₂O₂ effect (less than 2 days) was much shorter than that of AA (more than 30 days) because H₂O₂ was rapidly decomposed by either organic matter or metal ions (Figure 2f).

The rapid decomposition of H₂O₂ into water and oxygen is regarded as its great advantage over many other cyanocidal or cyanostatic substances in terms of environmental sustainability.¹⁰ However, the rapid decomposition of H₂O₂ also

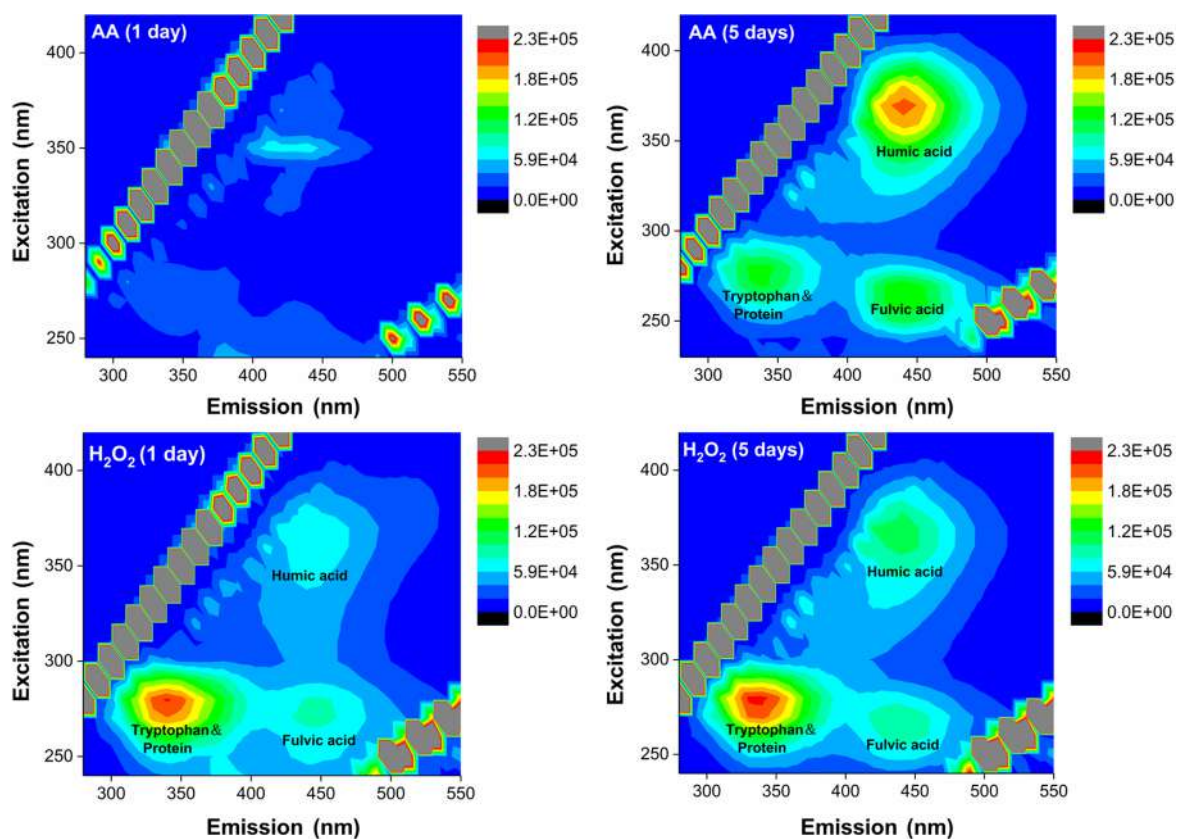


Figure 5. Extracellular organic matter (EOM) in AA- and H_2O_2 -incubated FACHB-905 cultures. The abundance of the EOM was reflected in the intensity of the fluorescence emission. The assignments of the peaks have been labeled near the peak centers.

brings significant disadvantages, since repeated treatment is needed to maintain its effective concentration. In many countries, e.g., in The Netherlands, the use of H_2O_2 is restricted to an upper limit of 5 mg L^{-1} .¹¹ In addition, the necessary and repeated addition of H_2O_2 increases the difficulty in its use: qualified and trained persons are required for the handling of concentrated H_2O_2 ($>10\%$ w/v). In comparison, AA is a stable chemical, which can be easily handled with normal operation.

Eco-safety of AA. AA has been mass-produced and used for centuries. For example, AA is employed as an additive in cosmetics to reduce the detrimental effects of UV radiation on human skin.²² On the basis of Henry's law, the estimated volatilization half-lives of AA in a model river and a model lake are 16 and 120 days, respectively.²³ According to the Regulation of the European Parliament and of the Council (# 1272/2008), AA is not hazardous to the aquatic environment. With a bioconcentration factor of 3.16, AA has been reported to have no risk for bioaccumulation (<https://echa.europa.eu/mt/registration-dossier/-/registered-dossier/14713/5/4/2>). The NOEC (i.e., no observed effect concentration) of AA for the early life stages of fathead minnow fish was reported to be 10 mg L^{-1} (<https://echa.europa.eu/mt/registration-dossier/-/registered-dossier/14713/6/2/3>), indicating that the dose of 10 mg L^{-1} of AA will not lead to long-term toxicity to fishes.

For a better understanding of the environmental implications of AA, *Lemna minor*, a species of duckweed that grows on the surface of water, was selected as a representative aquatic plant to check the cyanocidal selectivity of AA. To our surprise, AA had no harmful effect on *Lemna minor* up to 1000 mg L^{-1} ,

whereas H_2O_2 at a concentration of 68 mg L^{-1} led to significant negative effects on both the survival rate of the leaves and the content of Chl *a* (Figure S1). This result is consistent with the lower aquatic toxicity of AA (Table S1) in comparison to that of H_2O_2 (Table S3).

Physiological and Biological Status of AA-Incubated Cells. The occurrence of apoptosis has been consistently reported to be triggered by either a direct exogenous oxidant (e.g., H_2O_2) treatment or by indirect generation of internal reactive oxygen species (ROS) in *Microcystis* cells, although the detailed apoptotic pathway in *Microcystis* remains unknown and has yet to be explored.¹⁸ Our results suggest that apoptosis is not exclusively caused by oxidative stress; it could also be triggered by nonoxidative stress. The underlying mechanism warrants a further study.

In comparison to H_2O_2 , AA had a slower inhibition rate on the photosynthetic reactions in terms of both the effective quantum yield (Φ_e) and the maximum relative electron transport rate ($r\text{ETR}_{\text{max}}$) (Figure 3a); this is because AA was less effective for the destruction of membranes (Figure 3b and Figure S2). By an analysis of the cells with the Annexin V-FITC/PI apoptosis detection kit, two different modes were observed for the death of FACHB-905 cells: (i) apoptosis for the AA-incubated cells (84.1% at 36 h) and (ii) necrosis for the H_2O_2 -incubated cells (98.4% at 36 h) (Figure 3c).

The apoptosis of cells in the AA-treated culture was directly reflected by the disintegration of their thylakoids. As shown in Figure 3d, the cells of FACHB-905 have regularly organized thylakoid membrane lamella, uniformly distributed phycobilisomes (PBS) and carboxysomes, and filled cytoplasm regions. After incubation with AA for 3 days, the PBS and the

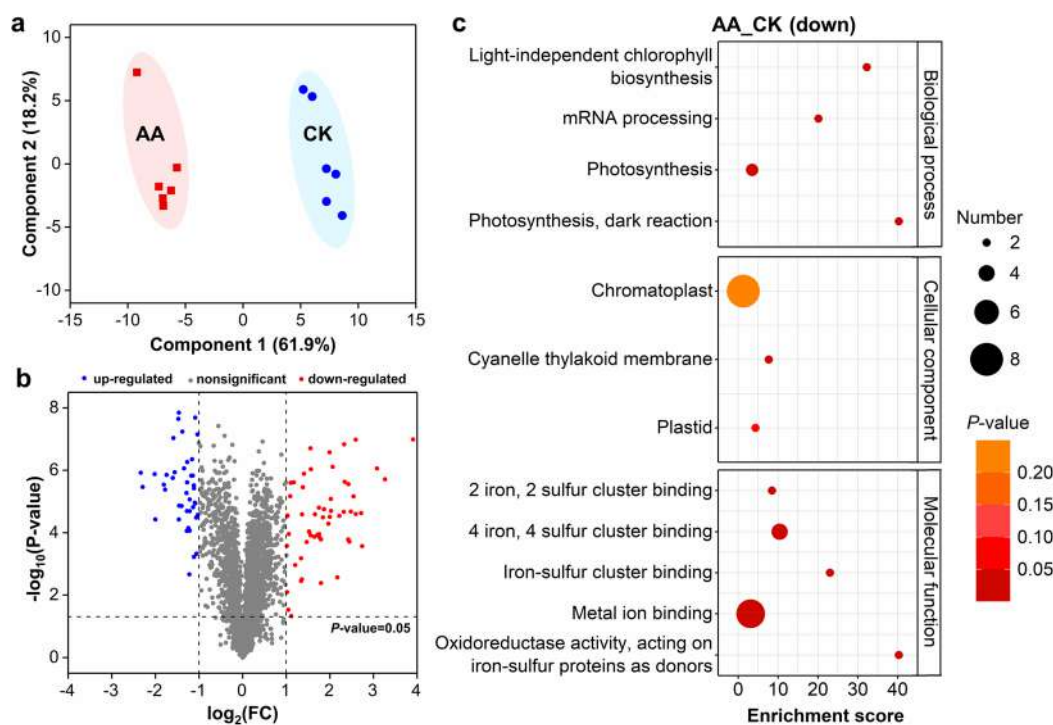


Figure 6. Metabolite analysis and proteomics assay. (a) Principal component analysis of metabolites in AA-incubated *Microcystis aeruginosa*. (b) Proteins in AA-incubated *Microcystis aeruginosa* identified in a proteomics assay with the screening criteria of fold change (FC) and significance level (P value). (c) The top 15 downregulated proteins in AA-incubated *Microcystis aeruginosa*, obtained from a proteomics assay. The size of the bubble reflects the number of differential proteins, and the color of the bubble shows the significance level (see right side of the figure). The samples were collected after 3 days of incubation with 0.1 mM of AA.

carboxysomes remained intact; however, the cytoplasm and the thylakoid membrane lamella were lost (Figure 3d). In contrast, the thylakoid membrane lamellae of the H_2O_2 -incubated cells were still intact even after 3 days, whereas the PBS, carboxysomes, and cytoplasm were almost absent within 6 h of incubation (Figure 3d).

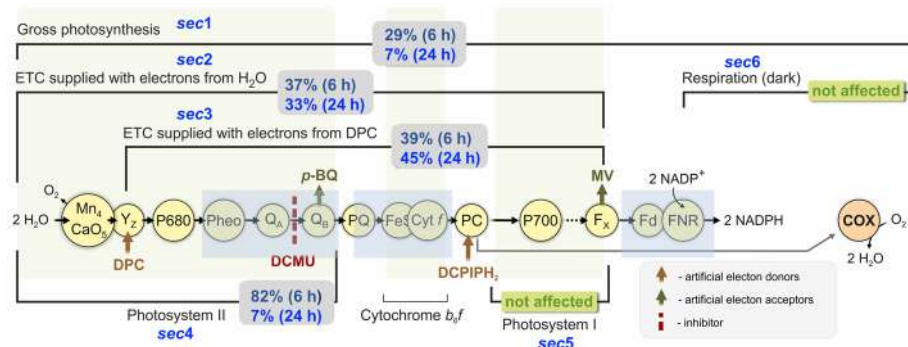
The above results were also supported by our observations on the content of all the three phycobiliprotein pigments, phycoerythrin (PE), phycocyanin (PC), and allophycocyanin (APC); their concentrations remained nearly unchanged up to 2 days in the AA-incubated cells. In contrast, the same pigments in the H_2O_2 -incubated cells showed a decline from the very beginning (Figure S3); this is because a high concentration level of ROS was generated by H_2O_2 , whereas that generated in the AA-incubated cells was at a very low level (Figure 4a). Consequently, higher concentrations of antioxidants, including superoxide dismutase (SOD), peroxidase (POD), and glutathione (GSH), as well as a lipid oxidation product, malondialdehyde (MDA), were observed in the H_2O_2 -incubated cells (Figure 4b), whereas the concentrations of both the antioxidants and MDA in the AA-incubated cells were only slightly higher than those in the controls (Figure 4b), suggesting that the inactivation caused by AA was not due to oxidative stress.

The death of cells ultimately led to the release of organic matter into the medium. The observed presence of MC-LR (the most common microcystin) in the medium is consistent with the conclusion about the death of the cells: the extracellular MC-LR appeared and built up earlier in the H_2O_2 -treated culture than in the AA-treated samples (Figure S4). The extracellular organic matter (EOM) in the H_2O_2 sample was mainly amino acids; their fluorescence spectra

changed only slightly from the second day to the fifth day (Figure 5). In contrast, the EOM in the AA sample mainly consisted of humic substances, which appeared much later: i.e., between day 1 and day 5 (Figure 5). We suggest that this was so because the oxidative breakage of the cells occurred more quickly in the H_2O_2 -treated samples.

The metabolites in AA-treated cells were significantly different from those of the controls (Figure 6a and the data files noted in the Acknowledgments), indicating that the metabolic pathways of the cells were altered by AA treatment. The main pathways affected by this treatment were those of the biosynthesis of amino acids and aminoacyl-tRNA, as well as the carbon fixation in photosynthesis and the tricarboxylic acid cycle (Figure S5). All the hits for gene ontology enrichment analysis are presented in Figure S6. Hundreds of proteins in the cells were either upregulated or downregulated (Figure 6b and Figure S7). The proteins for both the light-independent Chl biosynthesis and for the light-dependent photosynthesis were downregulated by AA. The significantly affected (downregulated) molecular functions are those related to the iron–sulfur cluster (Fe–S) binding, metal ion binding, and the oxidoreductase activity (Figure 6c). Under the differential screening criteria with a change of >2-fold, and a P value of <0.05 (see the Experimental Section), PetF and PetH (protein subunits in ferredoxin (Fd) and Fd-NADP⁺-oxidoreductase (FNR), respectively) were identified as the proteins of the photosynthetic electron transport chain (ETC) to have been affected by AA treatment (Figure S8).

Functional Mechanism of AA. Fd is the final electron acceptor of Photosystem I (PSI) in oxygenic photosynthesis; it binds to FNR *via* intermolecular electrostatic interactions.^{24,25} In the Fd-FNR complex, an Fe_2S_2 cluster is the redox center



Gross photosynthesis (**sec1**), ETC supplied with electrons from H₂O (**sec2**) or DPC (**sec3**), and PSII (**sec4**) were affected. PSI (**sec5**) and dark respiration (**sec6**) were not affected.

sec1 – sec2: There was significant difference at 24 h, indicating that PSI to Fd-FNR was affected.

sec2 – sec3: There was no significant difference, indicating that OEC was not affected.

sec2 – sec4: There was significant difference, indicating that Cyt_{b₆}f was affected.

Figure 7. Probing photosynthetic electron transport chain (ETC) and its different sections (labeled as *secX*) by measuring O₂ evolution/consumption rates using artificial electron donors and acceptors as well as specific inhibitors of electron carriers. The data in parentheses are the remaining oxygen evolution/consumption activities as a percent of control, R_{O₂}(%) (calculated as R_{O₂}(AA)/R_{O₂}(Ctrl) ratio), for the different sections in the photosynthesis ETC after 6 and 24 h incubation with 0.1 mM of AA. The R_{O₂} values are given in Table S6. Here, gross photosynthesis depicts both photosynthesis and respiration. The light blue shadow regions indicate the sections of ETC affected by AA.

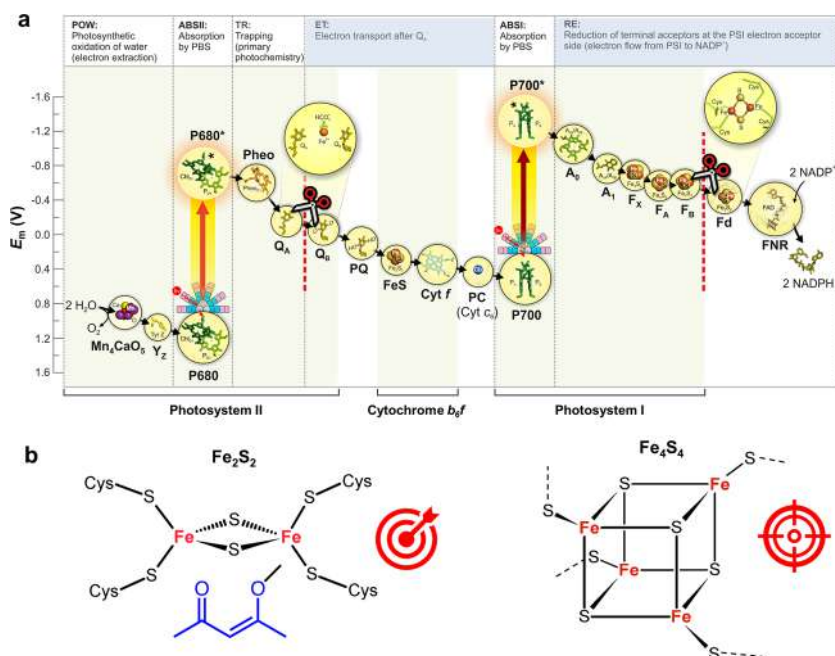


Figure 8. Action sites of acetylacetone (AA) in the photosynthetic electron transport chain (ETC). (a) The Z-scheme of photosynthetic electron transport (the Chl *a* containing light-harvesting antennas are not shown), modified from Govindjee et al.⁴⁰ E_m denotes the midpoint redox potential. The two scissors indicate the action sites of AA. The blue shadow regions on the top bar indicate the sections affected by AA (b) The iron–sulfur clusters suggested to be the binding sites of AA.

with a highly negative redox potential.^{26,27} This redox center catalyzes the formation of NADPH (the reduced form of nicotinamide adenine dinucleotide phosphate).²⁴ On the basis of a proteomics assay (Figure 6c), we conclude that the Fe–S center of Fd must be, at least, one of the functional sites that is “attacked” by AA.

To check the above conclusions, particularly on PSII, Chl *a* fluorescence transient curves were measured and analyzed by the so-called JIP test to identify the functional sites (Table S4 and Figure S9).^{28–33} These results imply that the rates of electron transport from Q_A to Q_B and the intersystem electron carriers, as well as to the terminal electron acceptors at the

acceptor side of PSI, were inhibited (see Text S2, Table S4, and Figure S9 for more details).

The above conclusion was further validated by probing the functionality of photosynthetic ETC *via* measurements of light-induced oxygen evolution/consumption reactions in our samples. After the addition of electron donors, inhibitors, and electron acceptors in different combinations (Table S5),^{34,35} oxygen evolution/consumption rates (R_{O₂}, in units of μmol of O₂ (mg of Chl *a*)⁻¹ h⁻¹) were measured (Figure S10 and Table S6). The remaining functional activities (R_{O₂}%) of the different sections of the photosynthetic ETC, labeled as *secX*,

after 6 and 24 h AA treatments are schematically shown in Figure 7. The R_{O_2} values of the ETC with electrons from H_2O , *sec2* (37% at 6 h and 33% at 24 h), and the ETC with electrons from diphenyl carbazide (DPC, an artificial electron donor), *sec3* (39% at 6 h and 45% at 24 h), were close, suggesting that the Mn_4CaO_5 cluster of the oxygen-evolving complex (OEC) was not affected by AA. However, the R_{O_2} value of gross photosynthesis (including both photosynthesis and respiration), *sec1* (29% at 6 h), was much lower than that of the PSII section, *sec4* (82% at 6 h), indicating that the damage occurred not only at PSII but also at some other site(s) somewhere in the photosynthetic ETC (such as the plastoquinone pool, cytochrome *b₆f*, PSI, Fd-FNR) and perhaps even respiration. However, no effect was observed on the R_{O_2} value of PSI (*sec6*) and on dark respiration (*sec5*) (Table S6 and Figure 7). The latter conclusion is supported by the long-term (5 days) incubation experiments, showing that AA had no inhibition effect on the growth of FACHB-905 if the culture was kept in darkness. Obvious differences were observed between *sec1* and *sec2* or *sec2* and *sec4*, suggesting that the electron transport was affected at the Fd site as well as in the section of intersystem electron carriers.

On the basis of the type of electron acceptors on the reducing (acceptor) side of the photosystems, the reaction centers (RCs) of the PSI and PSII core complexes have been classified as FeS-type RCs and Q-type RCs.³⁶ The FeS-type RCs contain Fe–S clusters that accept electrons from specific quinone cofactors. AA, due to its enol structure, is known to act as a ligand to about 60 metals, including Fe.³⁷ Both the metabolite (Figure 6c) and ETC (Figure 7) analyses confirmed that the Fe–S clusters, especially those related with oxidoreductase, are the action sites of AA. Therefore, it is highly reasonable to infer that AA binds to the Fe–S clusters of Fd, leading to the observed inhibition of photosynthesis.

On the other hand, in the Q-type RCs, there is a nonheme Fe flanked between Q_A and Q_B (Figure 8a). Nonheme Fe is also the active species in many oxidases and oxygenases. For example, the AA dioxygenase has a nonheme Fe center as the active site for the binding of AA.³⁸ In cyanobacteria, as in other oxygenic photosynthesizers, the nonheme Fe binds to two histidyl ligands and one bicarbonate (HCO_3^-) ligand.^{32,35,36} The bound HCO_3^- is thought to be essential for the efficient electron transfer from Q_A to Q_B and for the protonation reactions near the Q_B -binding site.^{39,40} Recent studies indicate that this HCO_3^- may not be a tightly bound ligand to the nonheme Fe under light conditions. The light-induced reduction of Q_A may lead to the release of HCO_3^- from its binding site on the nonheme Fe.^{41,42} AA is a much stronger ligand than HCO_3^- . Therefore, it is highly likely that AA binds to the nonheme Fe by replacing the HCO_3^- , thus leading to the subsequent inhibition of the electron transfer, followed by the inactivation of PSII. This possibility should be addressed by future studies.

To verify the above hypothesis, we incubated FACHB-905 cells with three other diketones: diacetyl (a simple α -diketone, whose chelating ability is much weaker than that of AA), AA-Cl (where one of the H atoms at the central carbon is replaced with chloride), and AA-(CH_3)₂ (where both of the H atoms at the central carbon are replaced with methyl groups) (Figure S11a). AA-Cl still could be isomerized to the enol structure and is, therefore, expected to have chelating ability. On the other hand, AA-(CH_3)₂ no longer has a chelating ability

because of the loss of the enol structure. Under otherwise identical conditions, both diacetyl and AA-(CH_3)₂ showed no inhibitory effect on the growth of FACHB-905 (Figure S11b), which justifies our hypothesis of photosynthetic inhibition by the binding of AA to the nonheme Fe and the Fe–S clusters in Fd.

We note that Fe–S clusters also exist in the intersystem electron carriers (Cyt *b₆f*) as well as in PSI (Figure 8a). It appears that AA has effects at the sites where bicarbonate is bound (see above) and near Cyt *b₆f* and Fd (Fe_2S_2 clusters), rather than at the terminal acceptors in PSI, i.e., the Fe_4S_4 centers of F_X , F_A , and F_B , for two possible reasons: (i) the existence of appropriate ligand spheres and/or (ii) matching of the midpoint redox potential (E_m).

Electrostatic forces and E_m are of major importance for the photosynthetic electron transport.⁴³ In comparison with the Fe in the Fe_4S_4 centers, the Fe in the Fe_2S_2 clusters is geometrically much more accessible to AA (Figure 8b). Moreover, the enhanced binding interaction, achieved through the development of a network of oppositely charged amino acids in the F_X and F_A/F_B proteins, provides protection for the Fe_4S_4 clusters.²⁷ The PsaA/PsaB proteins flank PsaC on either side of the stromal ridge of PSI, providing additional solvent shielding for F_A/F_B .²⁷ In contrast, the interactions between PSI and Fd are mainly due to electrostatic forces.^{24,27}

On complexation, the effects of AA on the Fe–S clusters were determined by the E_m values. It is highly possible that there is a threshold value of the E_m value for the ETC to be affected by AA. The E_m values of the Fe–S clusters are species-dependent, due to the different ligand environments.

In any case, the binding of AA with the Fe–S clusters is the prerequisite for the inhibitory action. Like E_m , the membrane permeability is also species-dependent. Therefore, it is reasonable to infer that the membrane permeability might set the first barrier for effectiveness, followed by the accessibility to the bound irons and the matching of E_m between AA and the attacked sites. The above factors might be able to explain the specific effects of AA on *Microcystis aeruginosa*, rather than *Lemma* and other organisms.

Environmental Implication. The reported cyanocides are generally derived from algicides. Many of the general algicides are known to inhibit photosynthesis by either binding at specific amino acid residues or generating oxidative stress.³⁶ As compared to these general algicides, AA functions in a quite different way: rather than generating oxidative stress, it works by binding to metals at specific sites. The special functional mechanisms make AA an ideal cyanocide for practical application in water bodies (target-selective, long-lasting, easily available, and eco-friendly).

Cyanobacteria are the primordial species that provide atmospheric molecular O_2 to Earth *via* photosynthetic oxidation of water.^{3,4} Although they have been extensively studied for a long time, questions on the evolution of their photosynthesis remain unanswered. For example, how cyanobacteria evolved the ability to oxidize H_2O and produce O_2 through photosynthesis is currently under discussion.^{3,44–46} The gated two-electron-transfer mechanism for the electron transport from Q_A to Q_B and the evolutionary role of bicarbonate in this process remain to be fully explored.³² Even the precise contributions of the known components in the photosystems need to be further evaluated.^{47,48} The interactions between AA and the photosynthetic proteins suggest a possible way to regulate the photosynthetic electron

transport, which may also provide important hints for the design of artificial photosynthesis.^{49,50}

■ ASSOCIATED CONTENT

SI Supporting Information

The Supporting Information is available free of charge at <https://pubs.acs.org/doi/10.1021/acs.est.1c04683>.

Experimental details, comparison with natural organic cyanocides, chlorophyll *a* fluorescence transient analysis, aquatic toxicity of AA, information on Sgnr and AA, acute aquatic toxicity of H₂O₂, chlorophyll *a* fluorescence parameters, information on the chemicals for the determination of oxygen evolution rates, dark respiration, rates of photosynthesis, and electron transport activity in *Microcystis aeruginosa*, effects of AA and H₂O₂ on the growth of *Lemna minor*, membrane integrity and cell status of AA- and H₂O₂-incubated FACHB-905, photosynthetic antenna pigments, evolution of MC-LR concentration, differential metabolic pathways, the GO categories of the differential proteins, top 15 proteins upregulated by AA, proteins in the photosynthetic electron transport chain, chlorophyll *a* fluorescence transient curves and key JIP-test parameters, the photosynthetic oxygen evolution, and molecular structures and algicidal performance of four diketones (PDF)

■ AUTHOR INFORMATION

Corresponding Author

Shujuan Zhang – State Key Laboratory of Pollution Control and Resource Reuse, School of the Environment, Nanjing University, Nanjing 210023, People's Republic of China; orcid.org/0000-0001-5013-5438; Phone: +86 25 8968 0389; Email: sjzhang@nju.edu.cn

Authors

Mihebai Yilimulati – State Key Laboratory of Pollution Control and Resource Reuse, School of the Environment, Nanjing University, Nanjing 210023, People's Republic of China

Jiyuan Jin – State Key Laboratory of Pollution Control and Resource Reuse, School of the Environment, Nanjing University, Nanjing 210023, People's Republic of China

Xin Wang – School of Life Science, Nanjing University, Nanjing 210023, People's Republic of China

Xiaomeng Wang – Resources and Environmental Sciences, Nanjing Agricultural University, Nanjing 210095, People's Republic of China; orcid.org/0000-0001-5058-4022

Dmitry Shevela – Department of Chemistry, Chemical Biological Centre, Umeå University, 90187 Umeå, Sweden; orcid.org/0000-0002-5174-083X

Bing Wu – State Key Laboratory of Pollution Control and Resource Reuse, School of the Environment, Nanjing University, Nanjing 210023, People's Republic of China; orcid.org/0000-0001-7117-580X

Kai Wang – Hansha Scientific Instruments Limited, Tai'an 271099, People's Republic of China

Lang Zhou – State Key Laboratory of Pollution Control and Resource Reuse, School of the Environment, Nanjing University, Nanjing 210023, People's Republic of China

Yunlu Jia – Institute of Hydrobiology, Chinese Academy of Sciences, Wuhan 430072, People's Republic of China

Bingcai Pan – State Key Laboratory of Pollution Control and Resource Reuse, School of the Environment, Nanjing University, Nanjing 210023, People's Republic of China; orcid.org/0000-0003-3626-1539

Govindjee Govindjee – Department of Biochemistry, Department of Plant Biology, and the Center of Biophysics & Quantitative Biology, University of Illinois at Urbana–Champaign, Urbana, Illinois 61801, United States

Complete contact information is available at: <https://pubs.acs.org/10.1021/acs.est.1c04683>

Author Contributions

○M.Y., J.J., and X.W. contributed equally to this paper.

Notes

The authors declare no competing financial interest.

■ ACKNOWLEDGMENTS

We thank Professors Changhong Liu, Han-Qing Yu, Jieshu Qian, and Shiguo Chen for discussions and their valuable input to this work. In addition, we thank Prof. Chunsheng Liu for his help in providing us the instrument for Chl *a* fluorescence transient measurements. D.S. is thankful to the Department of Chemistry at Umeå University for financial support. G.G. acknowledges constant support from the staff of the Life Sciences Office of Information Technology at the University of Illinois at Urbana–Champaign. This research was supported by the National Natural Science Foundation of China (22176087, 21976083) and the Key Technologies Research and Development Program of the Ministry of Science and Technology of the People's Republic of China (2018YFC1802003, 2019YFC0408302). We thank Shanghai LuMing Biological Technology Co., Ltd. (Shanghai, China) for providing omics services. The raw data of the omics analysis are available in a cloud disk at <https://box.nju.edu.cn/d/b02e413db27f4956a4e2/>.

■ REFERENCES

- (1) Kromdijk, J.; Glowacka, K.; Leonelli, L.; Gabilly, S. T.; Iwai, M.; Niyogi, K. K.; Long, S. P. Improving photosynthesis and crop productivity by accelerating recovery from photoprotection. *Science* **2016**, *354*, 857–861.
- (2) South, P. F.; Cavanagh, A. P.; Liu, H. W.; Ort, D. R. Synthetic glycolate metabolism pathways stimulate crop growth and productivity in the field. *Science* **2019**, *363*, eaat9077.
- (3) Soo, R. M.; Hemp, J.; Parks, D. H.; Fischer, W. W.; Hugenholtz, P. On the origins of oxygenic photosynthesis and aerobic respiration in Cyanobacteria. *Science* **2017**, *355*, 1436–1440.
- (4) Mishra, A.; Tiwari, D.; Rai, A. N. *Cyanobacteria: from Basic Science to Applications*; Academic Press: 2018.
- (5) Rastogi, R. P.; Madamwar, D.; Incharoensakdi, A. Bloom dynamics of cyanobacteria and their toxins: environmental health impacts and mitigation strategies. *Front. Microbiol.* **2015**, *6*, 1254–1276.
- (6) Huisman, J.; Codd, G. A.; Paerl, H. W.; Ibelings, B. W.; Verspagen, J. M. H.; Visser, P. M. Cyanobacterial blooms. *Nat. Rev. Microbiol.* **2018**, *16* (8), 471–483.
- (7) Ho, J. C.; Michalak, A. M.; Pahlevan, N. Widespread global increase in intense lake phytoplankton blooms since the 1980s. *Nature* **2019**, *574*, 667–670.
- (8) Plaas, H. E.; Paerl, H. W. Toxic Cyanobacteria: A growing threat to water and air quality. *Environ. Sci. Technol.* **2021**, *55*, 44–64.
- (9) Bullerjahn, G. S.; McKay, R. M.; Davis, T. W.; Baker, D. B.; Boyer, G. L.; D'Anglada, L. V.; Doucette, G. J.; Ho, J. C.; Irwin, E. G.; Kling, C. L.; Kudela, R. M.; Kurmayer, R.; Michalak, A. M.; Ortiz, J. D.; Otten, T. G.; Paerl, H. W.; Qin, B.; Sohngen, B. L.; Stumpf, R. P.;

- Visser, P. M.; Wilhelm, S. W. Global solutions to regional problems: Collecting global expertise to address the problem of harmful cyanobacterial blooms. A Lake Erie case study. *Harmful Algae* **2016**, *54*, 223–238.
- (10) Jancula, D.; Marsalek, B. Critical review of actually available chemical compounds for prevention and management of cyanobacterial blooms. *Chemosphere* **2011**, *85*, 1415–1422.
- (11) Matthijs, H. C. P.; Jančula, D.; Visser, P. M.; Maršálek, B. Existing and emerging cyanocidal compounds: new perspectives for cyanobacterial bloom mitigation. *Aquat. Ecol.* **2016**, *50*, 443–460.
- (12) Lushchak, V. I.; Matviishyn, T. M.; Husak, V. V.; Storey, J. M.; Storey, K. B. Pesticide toxicity: a mechanistic approach. *Excli J.* **2018**, *17*, 1101–1136.
- (13) Tan, K. T.; Huang, Z. Q.; Ji, R. B.; Qiu, Y. T.; Wang, Z. H.; Liu, J. X. A review of allelopathy on microalgae. *Microbiology* **2019**, *165*, 587–592.
- (14) Jin, J. Y.; Zhang, S. J.; Wu, B. D.; Chen, Z. H.; Zhang, G. Y.; Tratnyek, P. G. Enhanced photooxidation of hydroquinone by acetylacetone, a novel photosensitizer and electron shuttle. *Environ. Sci. Technol.* **2019**, *53*, 11232–11239.
- (15) Latifi, A.; Ruiz, M.; Zhang, C. C. Oxidative stress in cyanobacteria. *FEMS Microbiol. Rev.* **2009**, *33*, 258–278.
- (16) Chan, K. X.; Mabbitt, P. D.; Phua, S. Y.; Mueller, J. W.; Nisar, N.; Gigolashvili, T.; Stroehrer, E.; Grassl, J.; Arlt, W.; Estavillo, G. M.; et al. Sensing and signaling of oxidative stress in chloroplasts by inactivation of the SAL1 phosphoadenosine phosphatase. *Proc. Natl. Acad. Sci. U. S. A.* **2016**, *113*, E4567–E4576.
- (17) Schuurmans, J. M.; Brinkmann, B. W.; Makower, A. K.; Dittmann, E.; Huisman, J.; Matthijs, H. C. P. Microcystin interferes with defense against high oxidative stress in harmful cyanobacteria. *Harmful Algae* **2018**, *78*, 47–55.
- (18) Hu, C. L.; Rzymiski, P. R. Programmed cell death-like and accompanying release of microcystin in freshwater bloom-forming cyanobacterium microcystis: from identification to ecological relevance. *Toxins* **2019**, *11*, 706.
- (19) Omid, A.; Esterhuizen-Londt, M.; Pflugmacher, S. Interspecies interactions between *Microcystis aeruginosa* PCC 7806 and *Desmodesmus subspicatus* SAG 86.81 in a co-cultivation system at various growth phases. *Environ. Int.* **2019**, *131*, 105052.
- (20) Sandrini, G.; Piel, T.; Xu, T.; White, E.; Qin, H.; Slot, P. C.; Huisman, J.; Visser, P. M. Sensitivity to hydrogen peroxide of the bloom-forming cyanobacterium *Microcystis* PCC 7806 depends on nutrient availability. *Harmful Algae* **2020**, *99*, 101916–101929.
- (21) Cooper, W. J.; Zika, R. G. Photochemical formation of hydrogen peroxide in surface and ground waters exposed to sunlight. *Science* **1983**, *220*, 711–712.
- (22) Urbaniak, W.; Jurek, K.; Witt, K.; Goraczko, A.; Staniszewski, B.; Mickiewicz, A. Properties and application of diketones and their derivatives. *Chemik* **2011**, *65*, 273–282.
- (23) Lyman, W. J.; Reehl, W. F.; Rosenblatt, D. H. *Handbook of Chemical Property Estimation Methods*; American Chemical Society: 1990.
- (24) Kurisu, G.; Kusunoki, M.; Katoh, E.; Yamazaki, T.; Teshima, K.; Onda, Y.; Kimata-Aruga, Y.; Hase, T. Structure of the electron transfer complex between ferredoxin and ferredoxin-NADP⁺ reductase. *Nat. Struct. Biol.* **2001**, *8*, 117–121.
- (25) Aliverti, A.; Pandini, V.; Pennati, A.; de Rosa, M.; Zanetti, G. Structural and functional diversity of ferredoxin-NADP⁺ reductases. *Arch. Biochem. Biophys.* **2008**, *474*, 283–291.
- (26) Korn, A.; Ajlani, G.; Lagoutte, B.; Gall, A.; Sétif, P. Ferredoxin: NADP⁺ oxidoreductase association with phycocyanin modulates its properties. *J. Biol. Chem.* **2009**, *284*, 31789–31797.
- (27) Pierella Karlusich, J. J.; Carrillo, N. Evolution of the acceptor side of photosystem I: ferredoxin, flavodoxin, and ferredoxin-NADP⁺ oxidoreductase. *Photosynth. Res.* **2017**, *134*, 235–250.
- (28) Strasser, R. J.; Tsimilli-Michael, M.; Srivastava, A. Analysis of the Chlorophyll *a* Fluorescence Transient. In *Chlorophyll *a* Fluorescence: A Signature of Photosynthesis*; Papageorgiou, G. C., Govindjee, Eds.; Springer: 2004; pp 321–362.
- (29) Govindjee; Shevela, D. Adventures with cyanobacteria: a personal perspective. *Front. Plant Sci.* **2011**, *2*, 28.
- (30) Stirbet, A.; Govindjee. On the relation between the Kautsky effect (chlorophyll *a* fluorescence induction) and Photosystem II: Basics and applications of the OJIP fluorescence transient. *J. Photochem. Photobiol., B* **2011**, *104*, 236–257.
- (31) Stirbet, A.; Lazar, D.; Papageorgiou, G. C.; Govindjee Chlorophyll *a* Fluorescence in Cyanobacteria: Relation to Photosynthesis. In *Cyanobacteria: From Basic Science to Applications*; Mishra, A. N., Tiwari, D. N., Rai, A. N., Eds.; Academic Press: 2018; Chapter 5, pp 79–130.
- (32) Kalaji, H. M.; Jajoo, A.; Oukarroum, A.; Brestic, M.; Zivcak, M.; Samborska, I. A.; Cetner, M. D.; Lukasik, I.; Goltsev, V.; Ladle, R. J. Chlorophyll *a* fluorescence as a tool to monitor physiological status of plants under abiotic stress conditions. *Acta Physiol. Plant.* **2016**, *38*, 102–113.
- (33) Guo, Y. J.; Lu, Y. P.; Goltsev, V.; Strasser, R. J.; Kalaji, H. M.; Wang, H.; Wang, X. X.; Chen, S. G.; Qiang, S. Comparative effect of tenuazonic acid, diuron, bentazone, dibromothymoquinone and methyl viologen on the kinetics of Chl *a* fluorescence rise OJIP and the MR₈₂₀ signal. *Plant Physiol. Biochem.* **2020**, *156*, 39–48.
- (34) Chen, Z.; Juneau, P.; Qiu, B. S. Effects of three pesticides on the growth, photosynthesis and photoinhibition of the edible cyanobacterium *Ge-Xian-Mi* (Nostoc). *Aquat. Toxicol.* **2007**, *81*, 256–265.
- (35) Zhu, J. Y.; Liu, B. Y.; Wang, J.; Gao, Y. N.; Wu, Z. B. Study on the mechanism of allelopathic influence on cyanobacteria and chlorophytes by submerged macrophyte (*Myriophyllum spicatum*) and its secretion. *Aquat. Toxicol.* **2010**, *98*, 196–203.
- (36) Müh, F.; Zouni, A. The nonheme iron in photosystem II. *Photosynth. Res.* **2013**, *116*, 295–314.
- (37) Strydom, J.; Liljezin, J. O. Critical evaluation of equilibrium constants in solution. Stability constants of metal complexes. *Pure Appl. Chem.* **1982**, *54*, 2557–2592.
- (38) Park, H.; Bittner, M. M.; Baus, J. S.; Lindeman, S. V.; Fiedler, A. T. Fe(II) complexes that mimic the active site structure of acetylacetone dioxygenase: O₂ and NO reactivity. *Inorg. Chem.* **2012**, *51*, 10279–10289.
- (39) Shevela, D.; Eaton-Rye, J. J.; Shen, J.-R.; Govindjee. Photosystem II and the unique role of bicarbonate: a historical perspective. *Biochim. Biophys. Acta, Bioenerg.* **2012**, *1817*, 1134–1151.
- (40) Govindjee; Shevela, D.; Bjorn, L. O. Evolution of the Z-scheme of photosynthesis: a perspective. *Photosynth. Res.* **2017**, *133*, 5–15.
- (41) Brinkert, K.; De Causmaecker, S.; Krieger-Liszka, A.; Fantuzzi, A.; Rutherford, A. W. Bicarbonate-induced redox tuning in Photosystem II for regulation and protection. *Proc. Natl. Acad. Sci. U. S. A.* **2016**, *113*, 12144–12149.
- (42) Shevela, D.; Do, H. N.; Fantuzzi, A.; Rutherford, A. W.; Messinger, J. Bicarbonate-mediated CO₂ formation on both sides of Photosystem II. *Biochemistry* **2020**, *59*, 2442–2449.
- (43) Gorke, M.; Cherepanov, D. A.; Semenov, A. Y.; Golbeck, J. H. Control of electron transfer by protein dynamics in photosynthetic reaction centers. *Crit. Rev. Biochem. Mol. Biol.* **2020**, *55*, 425–468.
- (44) Najafpour, M. M.; Zaharieva, I.; Zand, Z.; Hosseini, S. M.; Kouzhanova, M.; Holyńska, M.; Tranca, I.; Larkum, A. W.; Shen, J. R.; Allakhverdiev, S. I. Water-oxidizing complex in Photosystem II: Its structure and relation to manganese-oxide based catalysts. *Coord. Chem. Rev.* **2020**, *409*, 213183.
- (45) Catling, D. C.; Zahnle, K. J. The archaic atmosphere. *Sci. Adv.* **2020**, *6*, eaax1420.
- (46) Oliver, T.; Sánchez-Baracaldo, P.; Larkum, A. W.; Rutherford, A. W.; Cardona, T. Time-resolved comparative molecular evolution of oxygenic photosynthesis. *Biochim. Biophys. Acta, Bioenerg.* **2021**, *1862*, 148400.
- (47) Lu, Y.; Gan, Q.; Iwai, M.; Alboresi, A.; Burlacot, A.; Dautermann, O.; Takahashi, H.; Crisanto, T.; Peltier, G.; Morosinotto, T.; Melis, A.; Niyogi, K. K. Role of an ancient light-

harvesting protein of PSI in light absorption and photoprotection.

Nat. Commun. **2021**, *12*, 679.

(48) Croce, R.; van Amerongen, H. Light harvesting in oxygenic photosynthesis: Structural biology meets spectroscopy. *Science* **2020**, *369*, eaay2058.

(49) Zhang, J. Z.; Reisner, E. Advancing photosystem II photo-electrochemistry for semi-artificial photosynthesis. *Nat. Rev. Chem.* **2020**, *4*, 6–21.

(50) Gaut, N. J.; Adamala, K. P. Toward artificial photosynthesis. *Science* **2020**, *368*, 587–588.

Regulation of Photosynthesis in Bloom-Forming Cyanobacteria with the Simplest β -Diketone

Mihebai Yilimulati^{1#}, Jiyuan Jin^{1#}, Xin Wang^{2#}, Xiaomeng Wang³, Dmitry Shevela⁴, Bing Wu¹, Kai Wang⁵, Lang Zhou¹, Yunlu Jia⁶, Bingcai Pan¹, Govindjee Govindjee⁷, Shujuan Zhang^{1*}

¹ State Key Laboratory of Pollution Control and Resource Reuse, School of the Environment, Nanjing University, Nanjing 210023, China

² School of Life Science, Nanjing University, Nanjing 210023, China

³ College of Resources and Environmental Sciences, Nanjing Agricultural University, Nanjing 210095, China

⁴ Department of Chemistry, Chemical Biological Centre, Umeå University, 90187 Umeå, Sweden

⁵ Hansha Scientific Instruments Limited, Tai'an 271099, China

⁶ Institute of Hydrobiology, Chinese Academy of Sciences, Wuhan 430072, China

⁷ Department of Biochemistry, Department of Plant Biology, and the Center of Biophysics & Quantitative Biology, University of Illinois at Urbana-Champaign, Urbana, IL 61801, USA

*Correspondence author. Phone: +86 25 8960389, E-mail: sjzhang@nju.edu.cn

Submitted to: *Environmental Science & Technology*

This file includes:

- (1) Texts S1 through S8;
- (2) Figures S1 through S11, with their legends;
- (3) Tables S1 through S6;
- (4) Supporting information references

Test S1. Chemicals and Materials

Lysine (Lys, 98%), ethyl 2-methylacetoacetate (EMA, > 95%), para-benzoquinone (*p*-BQ, \geq 99.5%), and bis-tris propane (BTP, 99%) were from Aladdin Industrial Corporation (Shanghai, China). Sanguinarine (Sgnr, 98%), Pyrogalllic acid (PA, 98%), 2,6-dichlorophenol indophenol (DCPIP, 97%), 3-(3',4'-dichlorophenyl)-1,1-dimethylurea (DCMU, 99%), methyl viologen (MV, 98%), N, N-diethyl-p-phenylenediamine (DPD, 98%), acetonitrile and formic acid of chromatographic grade were from Macklin Biochemical Technology Corporation (Shanghai, China). Anthraquinone (AQ, 99%), gallic acid (GA, 99%), 1,5-diphenylcarbazine (DPC), and ascorbic acid (Asc) were from Sinopharm Chemical Reagent Co., Ltd. (Shanghai, China). Peroxidase (POD, 99%) from horseradish was from Yuanye Biology Technology Co., Ltd. (Shanghai, China).

Text S2. Culturing and Sampling of *Microcystis aeruginosa* and *Lemna minor*

Two strains of *Microcystis aeruginosa*, toxic FACHB-905 and non-toxic FACHB-469, were obtained from the Freshwater Algae Culture Collection at the Institute of Hydrobiology, Chinese Academy of Sciences (Wuhan, China). The wild type *Lemna minor* was collected from a freshwater pond on the Campus of the Nanjing University (Nanjing, China).

The *Microcystis aeruginosa* culture reached logarithmic growth phase at approximately 20 days and was harvested for growth inhibition experiments with an initial cell density of 5×10^6 cells mL⁻¹. The cultivated cells of *Microcystis aeruginosa* and *Lemna minor* were further incubated under specific concentrations of AA, H₂O₂, or other chemicals.

Microcystis aeruginosa culture of 25 mL was sampled at specific time intervals, and centrifuged at $10528 \times g$ at 4°C for 5 min. The supernatant was directly subjected to analysis for AA and H₂O₂, extracellular organic matter (EOM), and extracellular microcystin-leucine-arginine (MC-LR). The precipitated cells were resuspended in 2 mL phosphate saline buffer (PSB) (pH 7.0, 50 mM) and washed with the same buffer three times for further analysis with transmission electron microscopy (TEM), pulse amplitude modulated (PAM) fluorescence measurements, and liquid-phase oxygen measurements to monitor the cell ultrastructure as well as their photosynthetic activity. The washed cells were resuspended either in PSB (for phycobilisomes, antioxidants, and oxidation products analysis), or in acetone/water mixture (90:10 v/v) (for Chl *a* analysis in *Microcystis aeruginosa*), or in ethanol/water (95:5 v/v) (for Chl *a* in *Lemna minor*). Samples were then frozen in liquid nitrogen and thawed at 4°C three times; the

suspensions were then centrifuged at $10528 \times g$ and 4°C for 5 min, and the supernatants, thus obtained, were filtered through a $0.22 \mu\text{m}$ polyether sulfone membrane for the analysis of Chl *a*.

Text S3. Analysis of Cell Structure, Membrane Integrity and Cell Viability

Microcystis aeruginosa cells, treated with Lugol's iodine, were counted at $400\times$ magnification with a hemocytometer, under a microscope (DMM-900C, Caikon Optical Instrumental Co., Ltd., China). The cell density was monitored at 680 nm (OD_{680}) with a double beam spectrophotometer (UV-2700, Shimadzu Co., Japan). A regression equation between OD_{680} (X) and the number of cells (Y , $\times 10^6$ cells/mL) was established as $Y = 25.561X + 0.3268$ ($R^2 = 0.99$).

For ultrastructure measurement, the washed cells were first fixed in 2.5% glutaraldehyde at 4°C overnight, postfixed in 1% osmium tetroxide for 2 h, dehydrated in a graded ethanol series (30%, 50%, 70%, 80%, 90%, 95%, and 100%), and then washed with tertbutyl alcohol and dried under vacuum; finally, the samples were embedded in an epoxy resin. Ultrathin sections (60-80 nm) of the cells were obtained using a diamond knife (EM FC7, Leica, Germany), after which the sections were stained with uranyl acetate and lead citrate for 15 min before measurement.

The cell integrity and viability of *Microcystis aeruginosa* were determined with a flow cytometer (FACS-Calibur, Becton Dickinson, USA) equipped with an air cooled 15 mW argon laser. First, washed cells in 1 mL PSB were mixed with 20 μL SYTOX green nucleic acid and then they were incubated at 25°C in darkness for 15 min.¹ Cells with intact cell membranes emit red (670 nm) fluorescence from phycoerythrin-Cy5 (PE-Cy5); this was recorded with the fluorescence channel 4 (FL4). On the other hand, cells with damaged cell membranes were stained with a green (530 nm) fluorescent dye (FITC) and recorded with the fluorescence channel 1 (FL1).

For the determination of the viability of the cells, *Microcystis* culture of 1 mL was first mixed with 200 μL Ca^{2+} binding buffer (10 mM 4-(2-hydroxyethyl)-1-piperazin ethane sulfonic acid/NaOH, pH 7.4, 140 mM NaCl, 2.5 mM CaCl_2), 5 μL Annexin V-FITC, and 5 μL propidium iodide (PI), and then the sample was incubated at 25°C in darkness for 15 min. Cells that were in early apoptosis are Annexin V-FITC positive and PI negative, emitting 530 nm fluorescence (FITC); we recorded it with the fluorescence channel 1 (FL1).² Cells that were in late apoptosis, or already dead, were positive for both Annexin V-FITC and PI, and gave 620 nm fluorescence (PI); this was recorded with the fluorescence channel 3 (FL3). Cells that were alive and not undergoing measurable apoptosis were negative for both Annexin V-FITC and PI, and they did not emit 530 nm or 620 nm fluorescence.

Text S4. Analysis of Cyanocides, Photosynthetic Pigments, Enzymes, and Metabolites

The concentration of AA was measured with high-performance liquid chromatography (HPLC).³ MC-LR was determined with an ultra-high performance liquid chromatograph system (UHPLC, U3000, Dionex, USA) coupled with a high-resolution Q Exactive Focus Orbitrap tandem Mass Spectrometer (MS/MS, Thermo Fisher Scientific, Germany). The UHPLC was equipped with a Hypersil Gold C8 column (100 mm × 2.1 mm, 3 μm; Thermo Fisher Scientific, USA). The mobile phase was a mixture of ultrapure water (with 0.1% formic acid) and acetonitrile (80:20 v/v) at a flow rate of 0.3 mL min⁻¹. MS signals were recorded with a heated electrospray ionization source operating in the positive ionization mode.

The amount of different phycobilin pigments was determined by measuring the absorbance of the supernatants at 565 nm, 620 nm, and 650 nm, respectively, for phycoerythrin (PE), phycocyanin (PC), and phycocyanin (APC) with a UV-vis spectrophotometer (UV-2700, Shimadzu Co., Japan) according to standard protocols for phycobiliprotein analysis.⁴ However, Chl *a* concentration was determined spectroscopically at 630, 645, 663 and 750 nm with the UV-2700 spectrophotometer.

The concentration of Chl *a* was calculated as follows:⁵

$$\text{Chl } a \text{ (}\mu\text{g/L)} = \frac{[11.64(A_{663}-A_{750})-2.16(A_{645}-A_{750})-0.10(A_{630}-A_{750})] \times V_1}{V} \quad (1)$$

where, A is the absorbance at the corresponding wavelength (cm⁻¹), V_1 is the volume of the tested extracting solution (mL), V is the sampling volume of the culture (L).

Further, the rate of decrease in Chl *a* concentration was calculated as follows:

$$\text{Inhibition rate (\%)} = \frac{[\text{Chl } a]_0 - [\text{Chl } a]}{[\text{Chl } a]_0} \times \% \quad (2)$$

where, $[\text{Chl } a]_0$ and $[\text{Chl } a]$ are the concentrations of Chl *a* in the control, and the treated sample, respectively.

For the quantification of ROS, washed cells in 1 mL PSB were added to the ROS assay kit and incubated at 37°C for 1 h. The suspension was then examined with a programmable microplate reader (Synergy H1M, BioTek, USA) at an excitation with 485 nm light and an emission at 525 nm. The relative fluorescence intensity of the treated samples with the control as the reference was used to quantify the amount of ROS produced.⁶

For the analysis of SOD,⁷ POD,⁸ MDA,⁹ and GSH,¹⁰ washed cells in 1 mL PSB were added to the ROS assay kit and incubated at 37°C for 1 h. The suspension was then examined with a programmable microplate reader (Synergy H1M, BioTek, USA) at an excitation with 485 nm and an emission at 525 nm.

The supernatants for SOD, POD, MDA, and GSH analysis were examined with the microplate reader at 450 nm, 420 nm, 532 nm, and 420 nm, respectively.

For the determination of SOD, POD, MDA, and GSH, the supernatants of lysed cells were added to the corresponding assay kits and were examined with the microplate reader at 450 nm, 420 nm, 532 nm, and 420 nm, respectively. The concentration levels were expressed as relative values with the control as the reference.

The fluorescence spectra of metabolites were recorded with a fluorescence spectrophotometer (Fluoromax-4, HORIBA Co., Germany) using excitation light in the range of 200 nm to 500 nm and emission from 250 nm to 550 nm.

Text S5. Monitoring of the Physiological Status of *Microcystis aeruginosa*

PAM (Pulse Amplitude Modulation) Analysis. This was done with cells immediately after they were harvested from the culture, but without dark adaption with the PHYTO-PAM phytoplankton analyzer (Walz, Germany). The effective quantum yield (Φ_e) for the photosynthesis of the *Microcystis* cells was calculated, using the following equation:

$$\Phi_e = (F_m' - F') / F_m' \quad (3)$$

where, F' and F_m' are the corresponding light-adapted steady-state Chl *a* fluorescence and light-adapted maximal Chl *a* fluorescence, respectively.

The maximal relative electron transport rate ($rETR_{max}$) was, however, calculated with a published method,¹¹ as follows:

$$rETR = \Phi_e \times PPFD \quad (4)$$

$$rETR = rETR_{max} \times (1 - e^{-\alpha \times I} / rETR_{max}) \quad (5)$$

where, PPFD is the photosynthetically active photon flux density, I is the intensity of the actinic light, and α is photosynthetic efficiency, determined by fitting the rapid light response curve to an exponential function, as modified from Platt et al.¹²

The JIP-test. The Chl *a* fluorescence transient curve, the OJIP curve, was recorded with the plant efficiency analyzer (Handy PEA, Hansatech, UK) in the time range of: 0.01-0.3 ms (per 10 μ s); 0.3-3 ms (per 100 μ s); 3-30 ms (per 1 ms); 30-300 ms (per 10 ms); and, 300-2000 ms (per 100 ms). The relevant parameters, calculated by the JIP-test,¹³⁻¹⁵ are presented in Table S4.

Oxygen Evolution. The rate of oxygen evolution was determined with the oxygen electrode setup (Oxytherm+R, Hansatech, UK) by recording the evolution of dissolved oxygen with time. The light

source was a xenon lamp (500 W) with a UV cut off filter ($\lambda > 400$ nm) at an intensity of 0.2 mW cm^{-2} . Cells of *Microcystis aeruginosa* were centrifuged at $1684 \times g$ for 4 min, and then suspended in a BG-11 medium with 25 mM bis-tris propane (BTP) buffer (pH 7.8). After 10 min of dark adaptation, the dark respiration rate was measured, while the photosynthetic rate was obtained when the samples were exposed to light. The types and concentrations of reagents used when measuring the various activities,^[34] described below, are provided in Table S5. The whole chain electron transport activity was estimated in NaN_3 -treated samples, as the uptake of oxygen with $\text{H}_2\text{O}/\text{DPC}$ as the electron donor, MV as the electron acceptor. Note that NaN_3 was used to inhibit respiration. The activity of PSII was measured by oxygen production with H_2O as the electron donor and *p*-BQ as the electron acceptor. PSI activity was determined by oxygen consumption in the presence of DCMU (that inhibits PSII activity), DCPIP H_2 (obtained by the reduction of DCPIP with Asc) as the electron donor, and MV as the electron acceptor. The rate of oxygen generation/consumption are presented in Table S6.

Text S6. Metabolite Analysis and Proteomics Assay

The cells after 3-day incubation with AA were collected after centrifugation, and then frozen at -80°C for metabolomics and proteomics assays. The metabolites and proteins were extracted from the frozen cells following standard published protocols.^{16,17}

A gas chromatograph (Agilent 7890B) equipped with a mass selective detector (Agilent 5977B, USA), with a DB-5MS fused-silica capillary column ($30 \text{ m} \times 0.25 \text{ mm} \times 0.25 \mu\text{m}$, Agilent, USA), was used to analyze the metabolites. Metabolites were unambiguously assigned by the BinBase identifier numbers, using the retention index and their mass spectra as the two most important identification criteria. Both unsupervised principal component analysis (PCA) and supervised partial least-squares-discriminant analysis (PLS-DA) were performed using online resources (<http://www.metaboanalyst.ca/>).

The proteins were digested with 1 mg mL^{-1} of tosyl-phenylalanine chloromethyl ketone treated trypsin¹⁷ and then the peptides were labeled using tandem mass tag (TMT) labeling kit (Thermo Fisher, USA). The labeled peptides were fractionated with a reverse-phase high-performance liquid chromatograph (Agilent 1100, USA) and a C18 column ($2.1 \text{ mm} \times 150 \text{ mm} \times 5 \mu\text{m}$, Agilent, USA) and then identified with MS/MS equipped with a nano-spray ionization source. The resulting MS/MS data were processed using the UniProt Taxonomy FASTA search engine.

The screening criteria used in this work for the selection of differential proteins are: fold change (FC) > 2 and significance level (*P*-value) < 0.05 ,¹⁸ where FC is a measure describing the degree of change in quantity between the final and original values. If the original value is X and the final value is Y, the

fold change is $(Y-X)/X$ or its equivalent $Y/X-1$ (<https://www.creative-proteomics.com/services/bioinformatic-fold-change-analysis-service.htm>).

Text S7. Performance Comparison with Natural Organic Cyanocides

To evaluate the cyanocidal effect of acetylacetone (AA) on *Microcystis aeruginosa* FACHB-905, experiments were conducted to compare its inhibitory effect with those of gallic acid (GA), pyrogallol (PA), anthraquinone (AQ), lysine (Lys), ethyl 2-methylacetoacetate (EMA), and sanguinarine (Sgnr) on *Microcystis aeruginosa* FACHB-905. The tested chemicals in this work were chosen from representative allelochemicals thus far reported for inhibition of the growth of algae.¹⁹⁻²¹ As shown in [Figure 2d](#) (see the main text), during the first 3 days of incubation, AA, GA, PA and Sgnr were the first to decrease the content of chlorophyll *a* (Chl *a*), which was followed by a similar effect by AQ and lysine. However, EMA showed no inhibitory effect on the growth of the cells. On the other hand, after 10 days of incubation with GA and PA, the cultures bloomed again ([Figure 2d](#)). Although AA, AQ, and Sgnr were the most effective, the cultures incubated with AQ and Sgnr were turbid. Further, AQ increased not only the turbidity but also the chromaticity of the medium. Sgnr is a broad-spectrum alkaloid type of antibiotic; its toxicity is comparable with those of other algicidal chemicals, such as copper sulphate and H₂O₂ (see the main text for reference).²² Except for the lack of selective toxicity (an order of magnitude more toxic to cyanobacteria than to other non-target species), Sgnr can be applied only in small amounts because of its high price (\$10,000–40,000 per ton).²²

Text S8. Analysis of Chlorophyll *a* Fluorescence Transient

The relationship between chlorophyll (Chl) *a* fluorescence and the electron transport chain of photosynthesis is shown in [Figure S9a](#) (see below). The definitions of the JIP parameters, including specific energy fluxes per reaction center (ABS/RC, DI₀/RC, TR₀/RC, ET₀/RC, RE₀/RC), quantum yields (ϕ_{P_0} , ϕ_{E_0} , ϕ_{R_0}), and probabilities (ψ_{E_0} , ψ_{R_0} , ψ_{R_0}) for various steps are provided in [Table S4](#) and in [Figure S9b](#). As shown in [Figure S9c](#), a faster rise in the J-step (i.e., O to J phase) was observed upon the addition of $\cong 7 \text{ mg L}^{-1}$ of AA, which is attributed to the accumulation of Q_A⁻.^{13,23} After a 41-h incubation with AA ($\cong 7 \text{ mg L}^{-1}$), the ET₀/RC and RE₀/RC values had decreased, whereas the ABS/RC and DI₀/RC values had increased, but the TR₀/RC remained nearly unchanged ([Figure S9d](#)). These results demonstrate that the trapped energy flux leading to Q_A reduction per RC at $t = 0$ was not affected, while the ensuing electron transport fluxes were inhibited.¹⁵ In parallel with the loss of electron transport

(decreased ET_0/RC and RE_0/RC), there was an increase in the dissipation of energy as heat (increased DI_0/RC); this was supported by the observation of up-regulated proteins for cellular response to heat (Figure S7). As demonstrated in Figure S3, the photosynthetic antenna was not significantly affected by AA in 2-day incubation. Therefore, the observed increase of ABS/RC (ratio of antenna Chl to RC Chl) demonstrates that the RCs must have been “destroyed”; this conclusion was supported by both the decreased RC/CS_0 (density of RCs to excited absorption cross section; see Figure S9d) and the decreased effective quantum yield (Φ_e) and the maximal relative electron transport rate ($rETR_{max}$; see Figure 3c).

To exclude the interference of data from possible dead cells, the JIP parameters of AA-treated samples within a 24 h-incubation were further analyzed (Figure S9e). In this period, most of the cells were still intact (Figure 3a). With only limited effects on the energy fluxes (ABS/RC , TR_0/RC and DI_0/RC), significant inhibition effects were observed in the rates and quantum yields, related to electron transport (ET_0/RC , RE_0/RC , ϕ_{E_0} , ϕ_{R_0} , ψ_0 , ψ_{R_0}). However, the ϕ_{P_0} was nearly unchanged, indicating that the primary photochemistry (reduction of pheophytin (Pheo) and of Q_A) was not affected. The decreased values of ϕ_{E_0} , ϕ_{R_0} , ψ_{E_0} and ψ_{R_0} demonstrate that the electron transport from the reduced Q_A to Q_B and the terminal electron acceptors at the PSI acceptor side were inhibited. As a result, the photosynthetic performance, as reflected by PI_{ABS} , was reduced. This was also reflected by the decreased fraction of Q_A reducing RCs (Figure S9e). The ϕ_{R_0} was slightly increased (Figure S9e), indicating that the electron transport from the intersystem electron carriers (PQ, Cyt *b₆f*, and PC) to the terminal electron acceptors at the PSI acceptor side was also affected.

Table S1. Aquatic toxicity of acetylacetone (AA) to various organisms in freshwater

Species	Condition	Toxicity	Concentration (mg L ⁻¹)	Exposure (hour)
Bluegill	flow-through	LC ₅₀	81	96
Bluegill	flow-through	LC ₅₀	60.1	96
Bluegill	flow-through	LC ₅₀	74.3	96
Bluegill	flow-through	LC ₅₀	77.9	72
Bluegill	flow-through	LC ₅₀	91.7	48
Bluegill	flow-through	LC ₅₀	155	24
Channel catfish	flow-through	LC ₅₀	155	48
Channel catfish	flow-through	LC ₅₀	83.6	96
Channel catfish	flow-through	LC ₅₀	106	96
Channel catfish	flow-through	LC ₅₀	83.6	72
Channel catfish	flow-through	LC ₅₀	106	96
Fathead minnow	lake water	LC ₅₀	200	24
Fathead minnow	flow-through	LC ₅₀	104	96
Fathead minnow	flow-through	LC ₅₀	142	96
Fathead minnow	flow-through	LC ₅₀	175	96
Goldfish	flow-through	LC ₅₀	133	72
Goldfish	flow-through	LC ₅₀	107	96
Goldfish	flow-through	LC ₅₀	155	48
Mosquitofish	flow-through	LC ₅₀	151	96
Rainbow trout	flow-through	LC ₅₀	81.6	48
Rainbow trout	flow-through	LC ₅₀	71.6	96
Rainbow trout	flow-through	LC ₅₀	92.4	96
Rainbow trout	flow-through	LC ₅₀	72.9	72
Rainbow trout	flow-through	LC ₅₀	101	24
Bullfrogs	flow-through	LC ₅₀	74	96
Bullfrogs	flow-through	LC ₅₀	156	96
Crayfish	flow-through	LC ₅₀	217	96
Crayfish	flow-through	LC ₅₀	631	96
<i>Gambusia affinis</i>	flow-through	LC ₅₀	177	96
<i>Gambusia affinis</i>	flow-through	LC ₅₀	204	96
<i>Daphnia magna</i>	static	EC ₅₀	75	48
<i>Daphnia magna</i>	static	EC ₅₀	47.6	48
<i>Daphnia pulex</i>	static	EC ₅₀	75	48
Green algae	flow-through	ErC ₅₀	300	24

Source: National Library of Medicine Hazardous Substances Data Bank (HSDB).

See the following web site:

<https://pubchem.ncbi.nlm.nih.gov/compound/31261#section=Ecotoxicity-Values&fullscreen=true> .

Abbreviations:

EC₅₀ is the effective concentration of a substance causing 50% of the maximum response.

ErC₅₀ is EC₅₀ in terms of reduction of growth rate.

LC₅₀ is the concentration of a chemical causing the death of 50% of a group of test animals.

EC₅₀, ErC₅₀ and LC₅₀ are the toxicity categories for crustacea, algae or other aquatic plants, and fishes, respectively.

These categories are defined by the Globally Harmonized System of Classification and Labelling of Chemicals (GHS) managed by the United Nations.

Table S2. Molecular weight, water solubility, and price of sanguinarine (Sgnr) and acetylacetone (AA)

Chemical	Molecular weight (g mol ⁻¹)	Water solubility	Purity	Price (US\$ kg ⁻¹)*
Sgnr	332.09	slightly soluble	98%	1158
			40%-60%	495
AA	100.11	16 g 100 mL ⁻¹	99%	26
			Industrial grade	0.6

* The median price, as searched online, on Dec 30, 2020 from:

https://www.chemicalbook.com/ProductList_En.aspx?kwd=Sanguinarine;

https://www.chemicalbook.com/ProductList_En.aspx?cbn=CB2179401

Table S3. Acute aquatic toxicity of hydrogen peroxide (H₂O₂) to various organisms in freshwater

Species	Chemical	Toxicity	Concentration (mg L ⁻¹)	Exposure (hour)
Bluegill sunfish	Hydrogen peroxide/Peroxyacetic acid (Divosan Forte)	LC ₅₀	20.7	96
Bluegill sunfish	Hydrogen peroxide/Peroxyacetic acid mixture	LC ₅₀	26.7	96
Bluegill sunfish	Hydrogen peroxide	LC ₅₀	150	96
Rainbow trout	Hydrogen peroxide/Peroxyacetic acid (Divosan Forte)	LC ₅₀	5	96
Rainbow trout	Hydrogen peroxide/Peroxyacetic acid mixture	LC ₅₀	22	96
Rainbow trout	Hydrogen peroxide	LC ₅₀	93	96
<i>Daphnia magna</i>	Hydrogen peroxide/Peroxyacetic acid (Divosan Forte)	EC ₅₀	4.3	48
<i>Daphnia magna</i>	Hydrogen peroxide/Peroxyacetic acid mixture	EC ₅₀	24	48
<i>Daphnia magna</i>	Hydrogen peroxide	EC ₅₀	24	48
<i>Daphnia pulex</i>	Hydrogen peroxide	EC ₅₀	2.4	48
<i>Daphnia pulex</i>	Hydrogen peroxide PAK 27 formulation	EC ₅₀	4.9	48
Duckweed	Hydrogen peroxide/Peracetic acid (Proxitane)	EC ₅₀	206	168
Blue-green algae	Hydrogen peroxide/Peracetic acid (Proxitane)	ErC ₅₀	1.5	96
Green algae	Hydrogen peroxide/Peracetic acid (Vigor Ox)	ErC ₅₀	0.18	120
Marine diatom	Hydrogen peroxide/Peracetic acid (Proxitane)	ErC ₅₀	27	96

Source: United States Environmental Protection Agency (US EPA) Pesticide Ecotoxicity Database. See:

<https://pubchem.ncbi.nlm.nih.gov/compound/784#section=EPA-Ecotoxicity&fullscreen=true>. EC₅₀

For definitions of LC₅₀, EC₅₀, and ErC₅₀, see the legends of Table S1.

Table S4. Chlorophyll *a* (Chl *a*) fluorescence parameters^{13-15*}

Chl <i>a</i> fluorescence parameters	Definition
F_t	Fluorescence at time t after the onset of actinic illumination
$F_O \cong F_{20 \mu s}$	Minimal fluorescence, when all the PSII reaction centers (RCs) are open
$F_K \equiv F_{300 \mu s}$	Fluorescence intensity at the K-step (300 μs) of the OJIP curve
$F_J \equiv F_{2 ms}$	Fluorescence intensity at the J-step (2 ms) of OJIP curve
$F_I \equiv F_{30 ms}$	Fluorescence intensity at the I-step (30 ms) of OJIP curve
$F_M = F_P$	Maximal recorded fluorescence intensity at the P-step when all the RCs are closed
$F_V = F_M - F_O$	Maximal variable fluorescence
$V_t = (F_t - F_O)/(F_M - F_O)$	Relative variable fluorescence at time t
$V_J = (F_J - F_O)/(F_M - F_O)$	Relative variable fluorescence at the J-step
$V_I = (F_I - F_O)/(F_M - F_O)$	Relative variable fluorescence at the I-step
$M_0 \equiv 4(F_{270 \mu s} - F_O) \times (F_M - F_O)$	Approximated initial slope of the fluorescence transient, related to the rate of closure of RCs
Specific energy fluxes (per active, i.e., Q_A-reducing PSII RC)	
$ABS/RC = M_0 \times (1/V_J) \times (1/\phi_{P0})$	Absorption flux per RC corresponding directly to its apparent antenna size–ratio between chlorophyll in antenna and chlorophyll in RC
$DI_0/RC = ABS/RC - TR_0/RC$	Dissipated energy flux per RC at the initial moment of the measurement (at $t = 0$)

$$TR_0/RC = M_0 \times (1/V_J)$$

Trapped energy flux leading to Q_A reduction per RC at $t = 0$

$$ET_0/RC = M_0 \times (1/V_J) \times (1-V_I)$$

Electron transport flux from Q_A^- to plastoquinone per RC at $t = 0$

$$RE_0/RC = M_0 \times (1/V_J) \times (1-V_I)$$

Electron transport flux from Q_A^- to the PS I end electron acceptors per RC at $t = 0$

Density of reaction centers

$$RC/CS_0 = \varphi_{P_0} \times (V_J/M_0) \times F_0$$

Density of active PSII RCs per excited cross section (CS)

$$Q_A \text{ reducing RC} = \frac{(RC/CS)_{\text{sample}}}{(RC/CS)_{\text{control}}} \cdot \frac{(ABS/CS)_{\text{sample}}}{(ABS/CS)_{\text{control}}}$$

Quantum efficiencies and probabilities

$$\varphi_{P_0} = TR_0/ABS = F_V/F_M$$

Maximum quantum yield of primary PSII photochemistry at $t = 0$

$$\varphi_{E_0} = ET_0/ABS = (1 - F_J/F_M)$$

Quantum yield for electron transport from Q_A^- to plastoquinone at $t = 0$

$$\varphi_{R_0} = RE_0/ABS = (1 - F_I/F_M)$$

Quantum yield for reduction of end electron acceptors at the PSI acceptor side at $t = 0$

$$\psi_{E_0} = ET_0/TR_0 = 1 - V_J$$

Probability (at $t = 0$) that a trapped exciton moves an electron from Q_A^- to plastoquinone

$$\psi_{R_0} = RE_0/TR_0 = 1 - V_I$$

Probability (at $t = 0$) that a trapped exciton moves an electron into the electron transport chain beyond Q_A^-

$$\delta_{R_0} = RE_0/ET_0 = (1 - V_I)/(1 - V_J)$$

Probability (at $t = 0$) of an electron transfers from the intersystem electron carriers to end electron acceptors at the PSI acceptor side

$$\gamma_{RC} = \frac{RC}{ABS + RC}$$

Probability that a PSII Chl *a* molecule functions as RC

Performance index, in terms of absorption

$$PI_{\text{ABS}} = \frac{\gamma_{\text{RC}}}{1 - \gamma_{\text{RC}}} \cdot \frac{\varphi_{\text{P0}}}{1 - \varphi_{\text{P0}}} \cdot \frac{\psi_{\text{E0}}}{1 - \psi_{\text{E0}}} \quad \text{Potential for energy conservation from photons absorbed by PSII to the reduction of intersystem electron acceptors}$$

Table S5. The type and concentration of chemicals added (with symbol “+”) for the determination of oxygen evolution rate^{24,25*}

	DPC	DCMU	<i>p</i> -BQ	DCPIP	Asc	MV	NaN ₃
Electron transport chain (ETC) ^a	(0.5 mM)	(10 μM)	(1 mM)	(0.1 mM)	(5 mM)	(0.1 mM)	(1 mM)
Gross photosynthesis (whole chain)							
ETC from H ₂ O (H ₂ O → MV)						+	+
ETC from DPC (DPC → MV)	+					+	+
PSII activity (H ₂ O → <i>p</i> -BQ)			+				
PSI activity (DCPIP → MV)		+		+	+	+	

DPC: 1,5-diphenylcarbazide; DCMU: 3-(3',4'-dichlorophenyl)-1,1-dimethylurea; *p*-BQ: para-benzoquinone; DCPIP: 2,6-dichlorophenol indophenol; Asc: ascorbic acid, used to reduce DCPIP to DCPIPH₂; MV: methyl viologen.

^a Gross photosynthesis depicts both photosynthesis (O₂ release in light) and respiration (O₂ uptake in dark). ETC from H₂O or DPC is for the electron transport chain with electrons from H₂O or DPC. The difference between ETC from H₂O and ETC from DPC reflects the role of oxygen-evolving complex (OEC) center.

Table S6. The dark respiration, rates of photosynthesis and electron transport activity in *Microcystis aeruginosa*. Control: in the absence of AA, AA: incubated with 10 mg L⁻¹ of AA, incubation time: 6 h and 24 h. The symbol “-” before the data means a negative rate of O₂ evolution (i.e., the uptake of O₂ outweighs the release of O₂).

Electron transport chain (ETC)	Rate (μmol O ₂ mg (Chl <i>a</i>) ⁻¹ h ⁻¹)			
	Control (6 h)	AA-incubated (6 h)	Control (24 h)	AA-incubated (24 h)
Dark respiration	-10.0 ± 0.5	-8.0 ± 2.0	-13.4 ± 2.9	-11.9 ± 4.5
Gross photosynthesis	204.8 ± 19.0	59.8 ± 1.6	282.1 ± 28.2	-18.5 ± 4.8
ETC from H ₂ O (H ₂ O → MV)	-119.7 ± 5.3	-44.5 ± 6.3	-129.4 ± 9.1	-43.3 ± 7.8
ETC from DPC (DPC → MV)	-151.9 ± 11.0	-59.1 ± 2.2	-185.8 ± 10.3	-84.1 ± 10.8
PSII activity (H ₂ O → <i>p</i> -BQ)	287.8 ± 20.8	237.3 ± 11.2	355.3 ± 11.5	23.9 ± 5.7
PSI activity (DCPIP → MV)	-73.3 ± 4.4	-68.8 ± 2.0	-58.2 ± 3.9	-56.6 ± 7.5

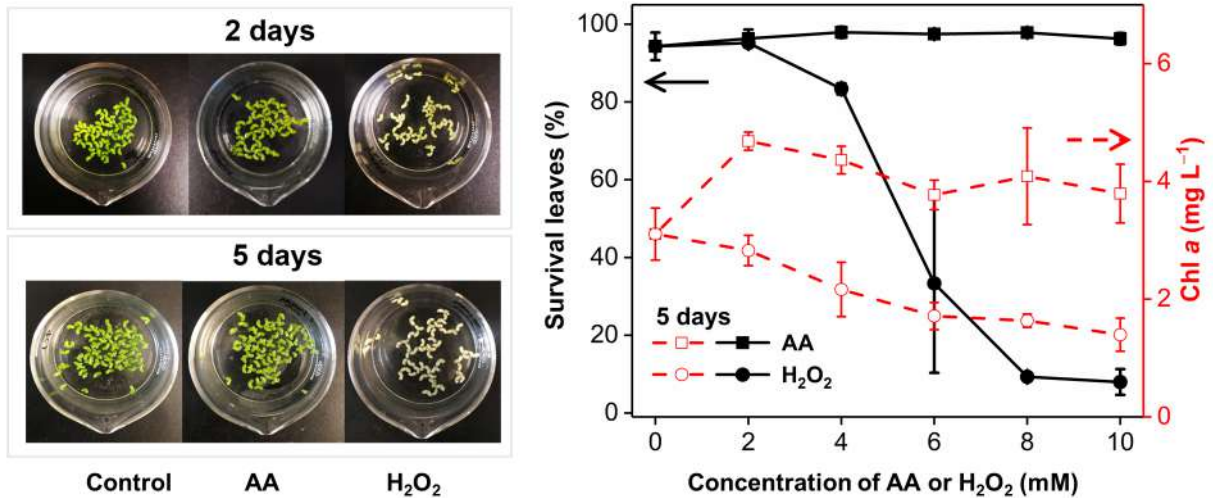


Figure S1. Effects of acetylacetone (AA) and H₂O₂ on the growth of *Lemna minor*. (left) A photograph of AA- and H₂O₂-treated strains of *Lemna minor*, (right) Chl *a* concentration (red curves) and the survival rate (black curves) of the leaves.

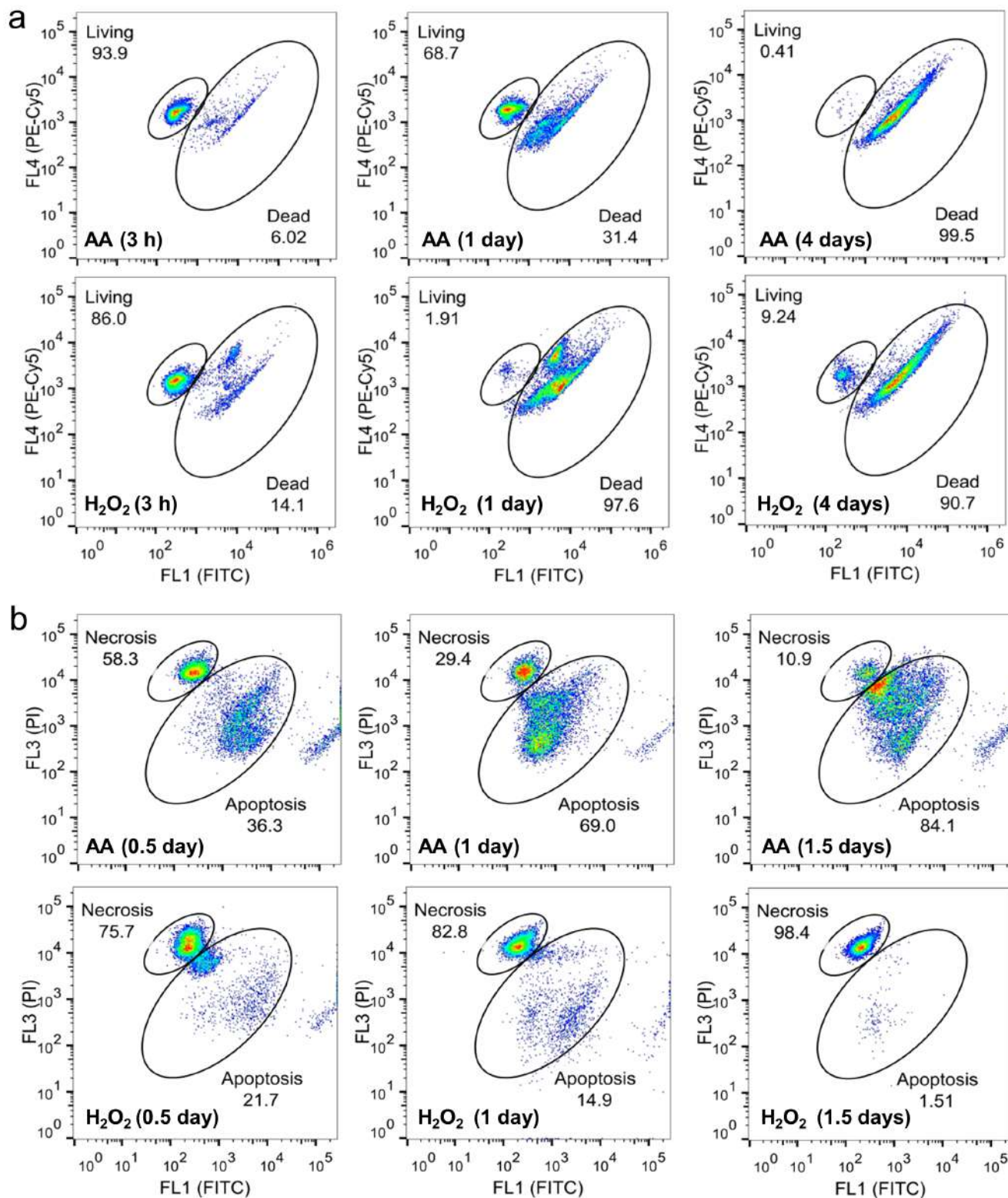


Figure S2. Membrane integrity and cell status of AA- and H₂O₂- incubated FACHB-905 cells. a, Membrane integrity determined with the SYTOX green nucleic acid staining;¹ b, Cell status determined

with the Annexin V-FITC apoptosis detection kit.² FITC: fluorescein isothiocyanate; PE-Cy5: Phycoerhthrin-Cy5; PI: propidium iodide; FL: fluorescence channels in flow cytometry. AA and H₂O₂: 0.1 mM.

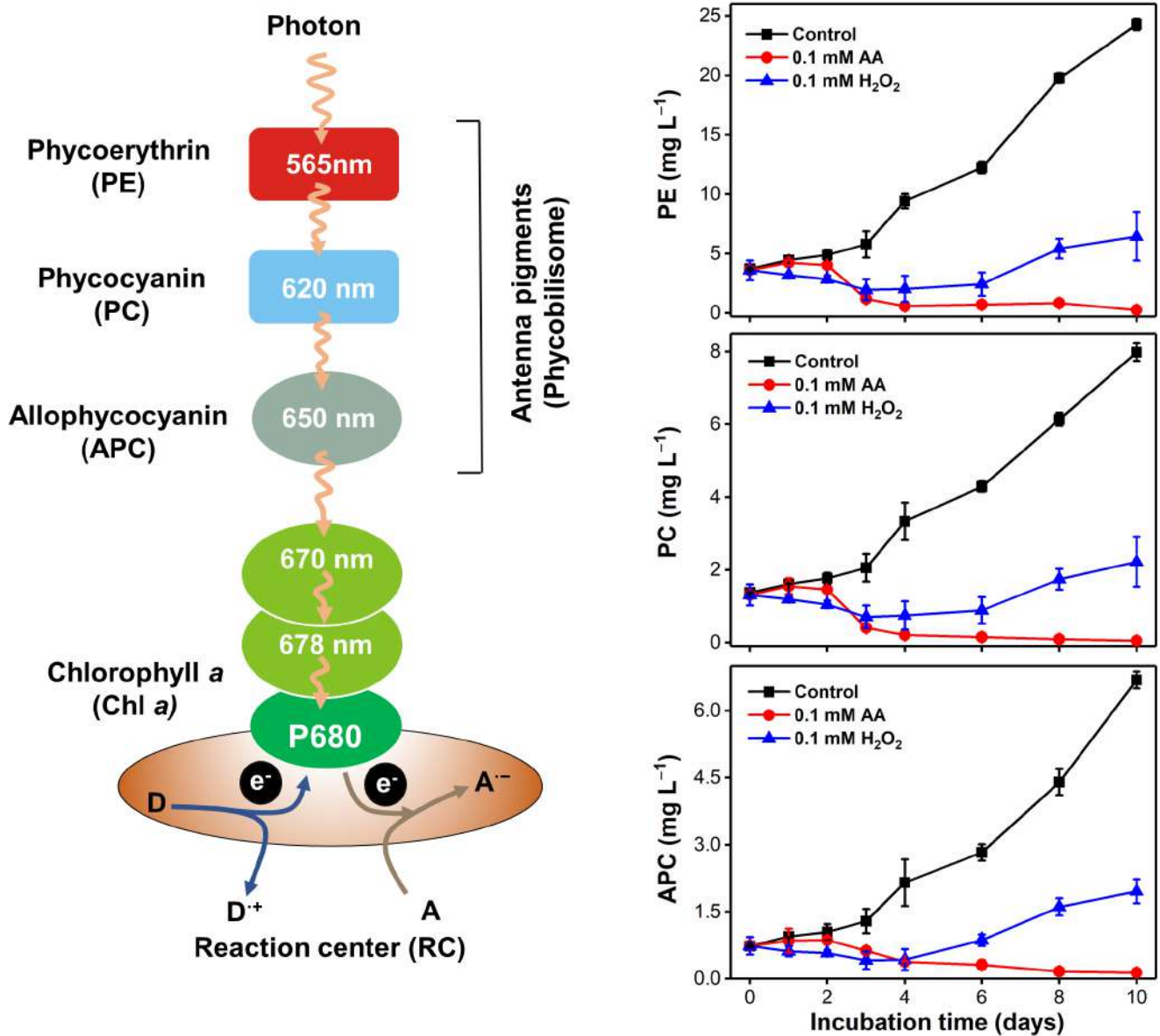


Figure S3. Photosynthetic antenna pigments. Left, The energy flux in photosynthetic antenna pigments. PSI and PSII share the same antenna pigments [shown here is PSII, which uses P680 as its reaction center Chl *a*]; Right, the concentration of phycoerythrin (PE), phycocyanin (PC), and allophycocyanin (APC) with incubation time in AA- and H₂O₂-incubated cultures of FACHB-905. Other abbreviations: D, primary electron donor; A, primary electron acceptor.

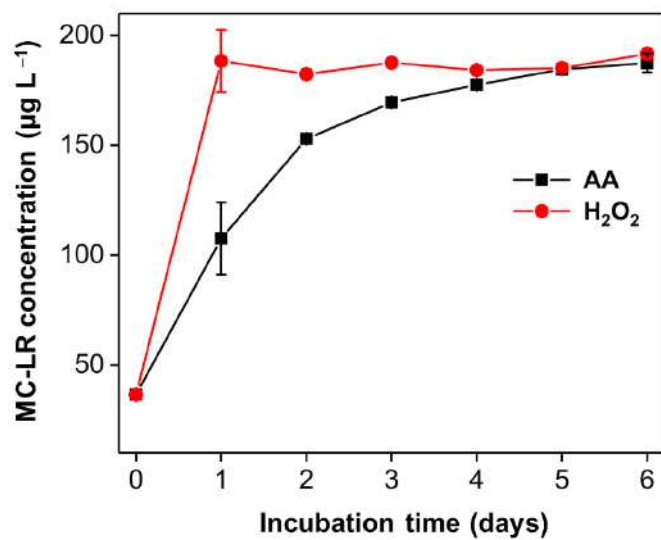


Figure S4. The extracellular microcystin-leucine-arginine (MC-LR) concentration in AA- and H_2O_2 -incubated cultures of FACHB-905. AA and H_2O_2 : 0.1mM.

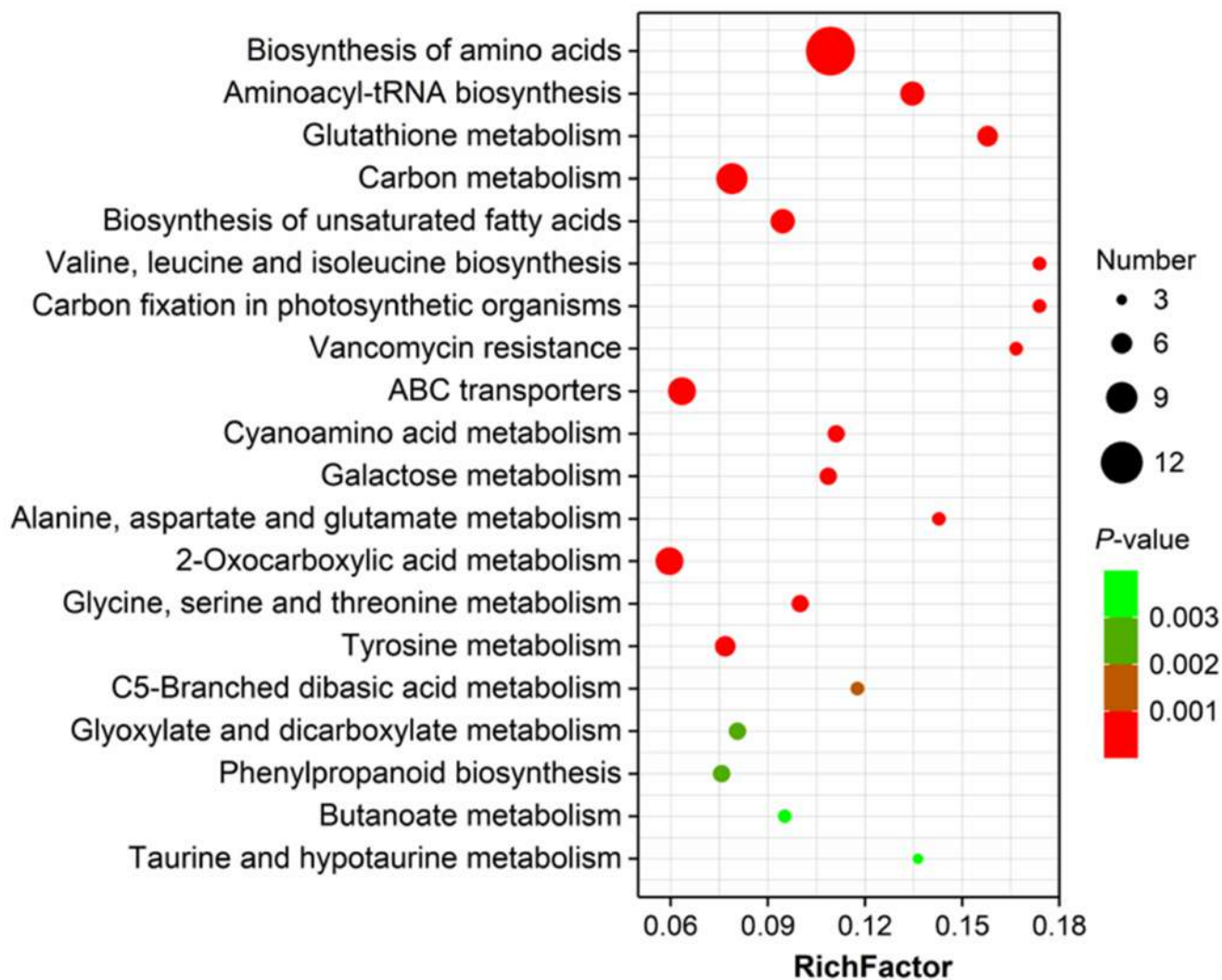


Figure S5. The top 20 differential metabolic pathways in AA-incubated FACHB-905. Components were identified by metabolite analysis using published protocols¹⁶ with the screening criterion of significance level (P -value) < 0.003 . The size of the bubble shows the number of differential metabolites. The color of the bubble shows the significance level. The samples were collected after 3 days of incubation with 10 mg L^{-1} of AA.

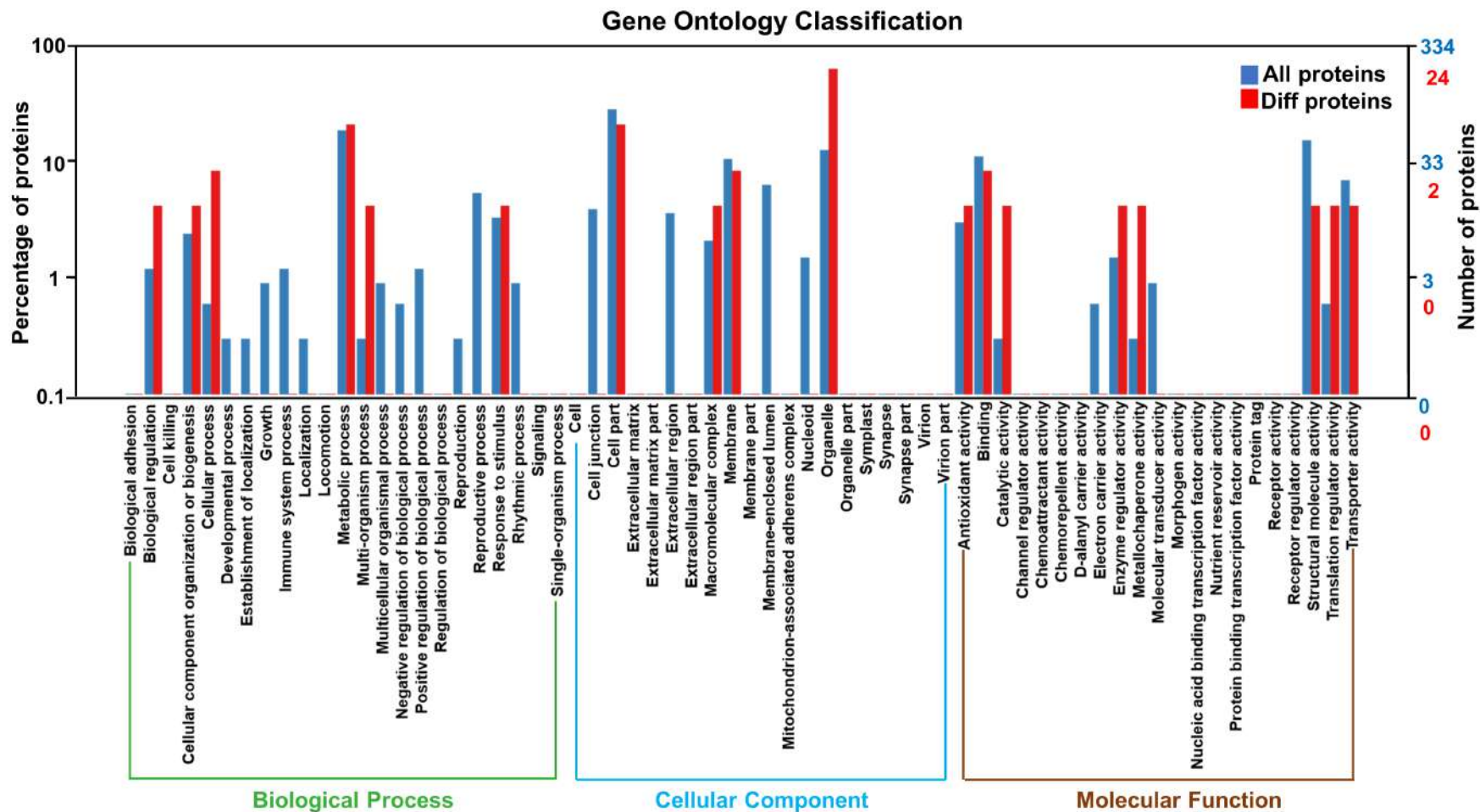


Figure S6. The gene ontology (GO) categories of the differential proteins. The blue bars represent all the enriched entries of species proteins at GO level 2. The red bars represent the enriched entries of differential proteins at GO level 2.

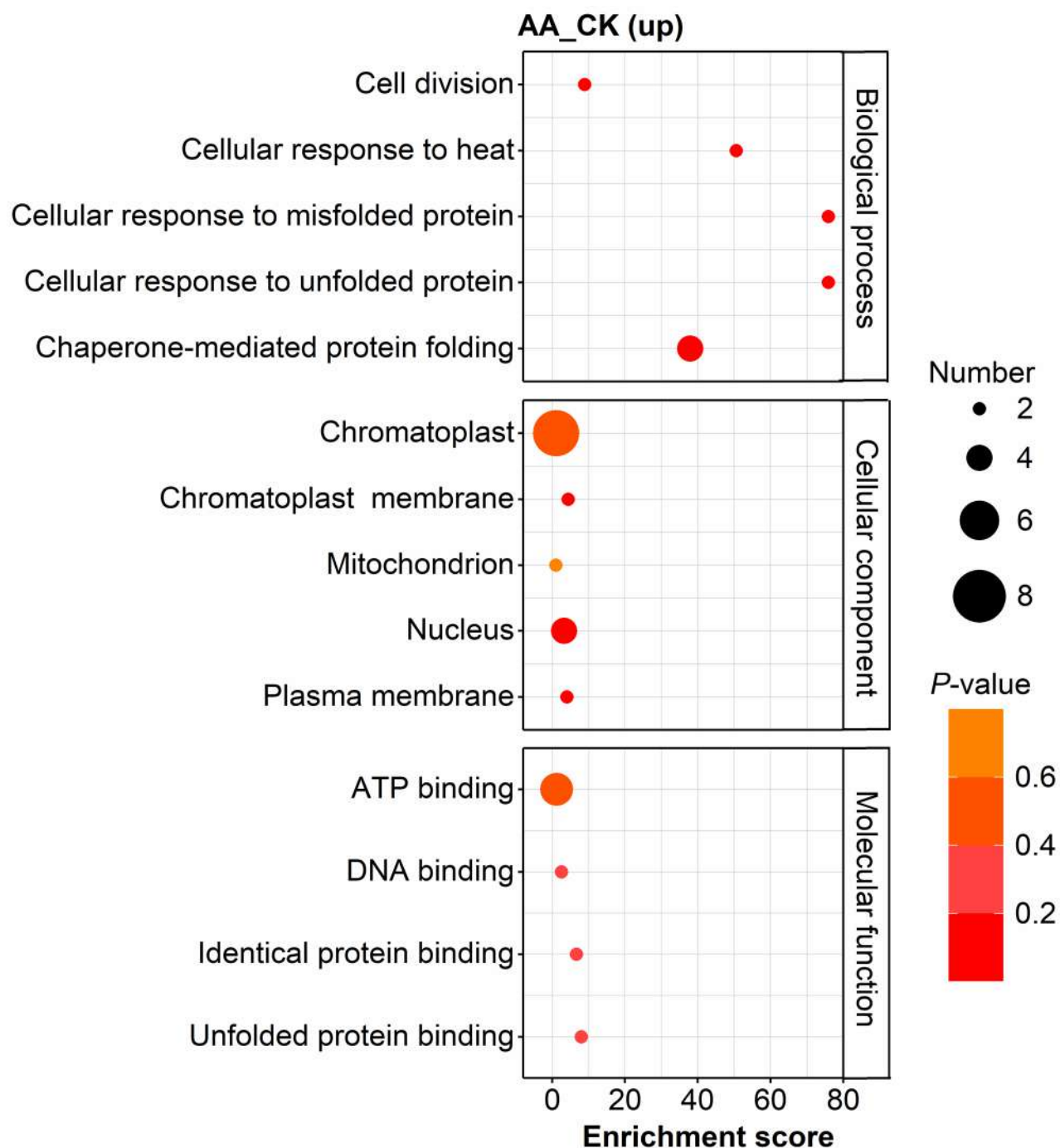
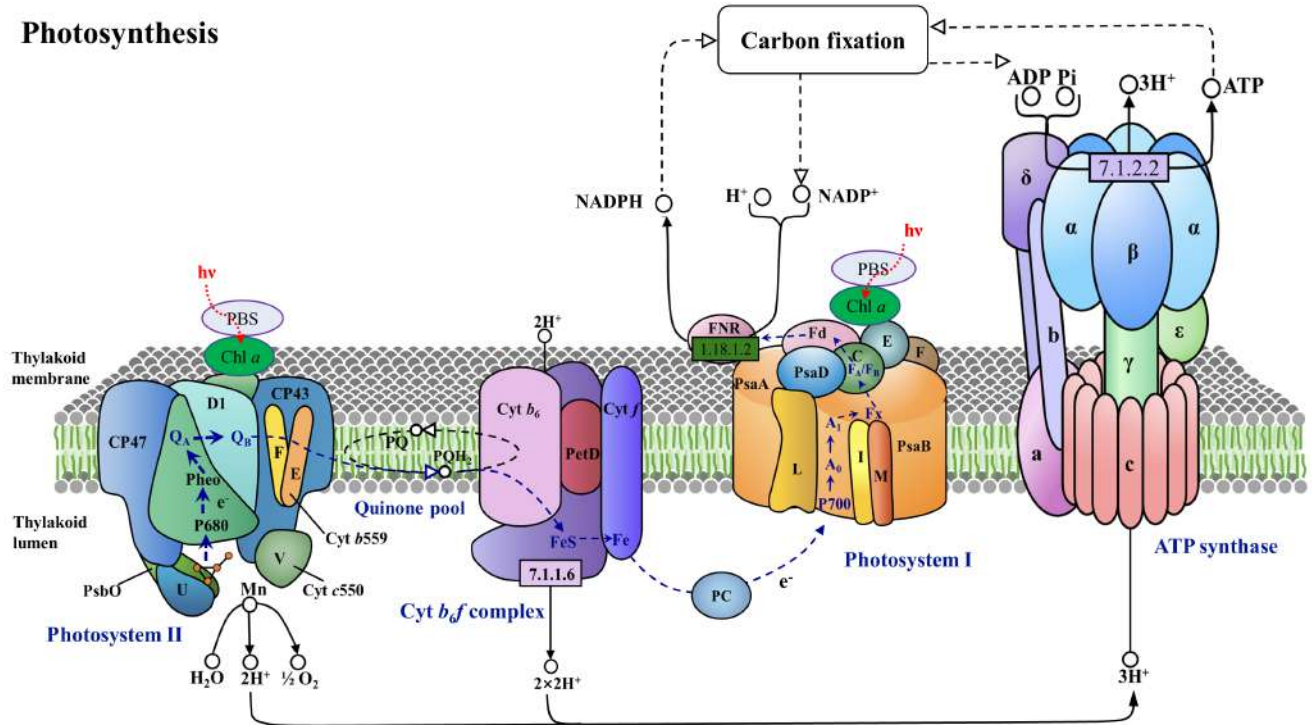


Figure S7. The top 15 proteins that were up-regulated by AA in the incubated culture of FACHB-905. Components were identified by proteomics assay, with published protocols.¹⁷ The size of the bubble shows the number of differential proteins. The color of the bubble shows the significance level. The samples were collected after 3 days of incubation with 10 mg L⁻¹ of AA. AA: acetylacetone. CK: control.

Photosynthesis



Photosystem II

D1	D2	CP43	CP47	Cyt <i>b</i> 559	
PsbA	PsbD	PsbC	PsbB	PsbE	PsbF

						MSP	OEC
PsbL	PsbJ	PsbK	PsbM	PsbH	PsbI	PsbO	PsbP
PsbQ	PsbR	PsbS	PsbT	PsbU	PsbV	PsbW	PsbX
PsbY	PsbZ	Psb27	Psb28	Psb28-2			

Photosystem I

PsaA	PsaB	PsaC	PsaD	PsaE	PsaF	PsaG	PsaH
PsaI	PsaJ	PsaK	PsaL	PsaM	PsaN	PsaO	PsaX

Cytochrome *b*₆*f* complex

PetB	PetD	PetA	PetC	PetL	PetM	PetN	PetG
------	------	------	------	------	------	------	------

Photosynthetic electron transport

PC	Fd	FNR	Cyt <i>c</i> 6
PetE	PetF	PetH	PetJ

F-type ATPase

α	β	γ	δ	ϵ	a	b	c
----------	---------	----------	----------	------------	---	---	---

Figure S8. Proteins in the photosynthetic electron transport chain, modified from the following website: https://www.kegg.jp/kegg-bin/show_pathway?map00195. Ferredoxin (Fd) and Fd-NADP⁺-oxidoreductase (FNR) were the two affected (down-regulated) proteins under the differential screening criteria of fold change > 2 and *P*-value < 0.05 in AA-treated samples (AA: 10 mg L⁻¹, incubation time: 3 days).

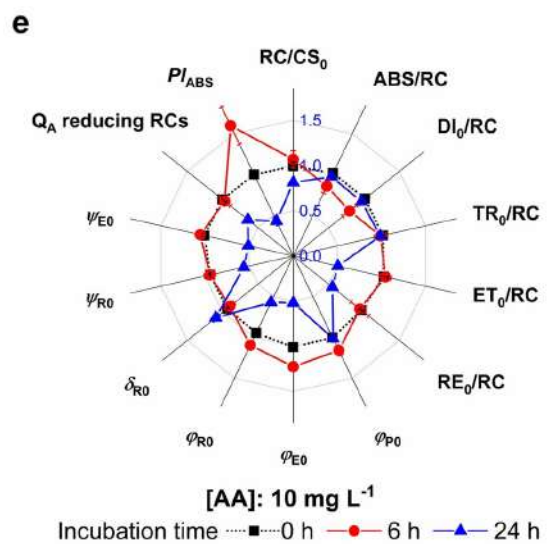
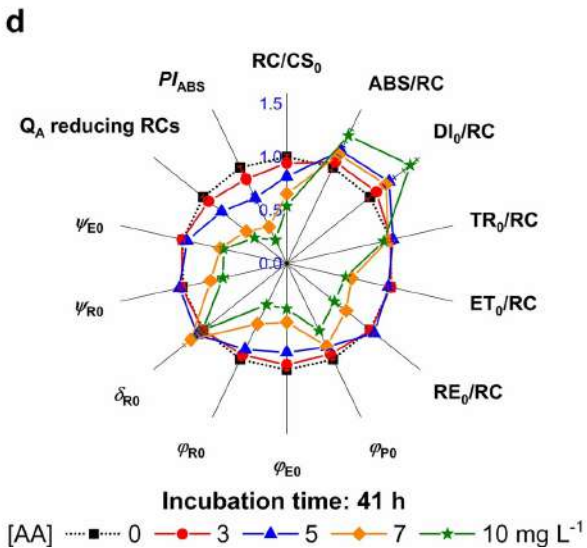
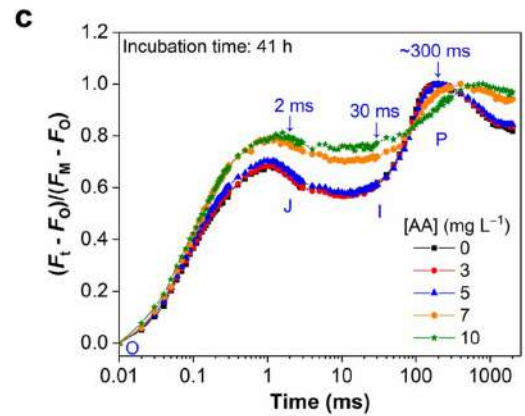
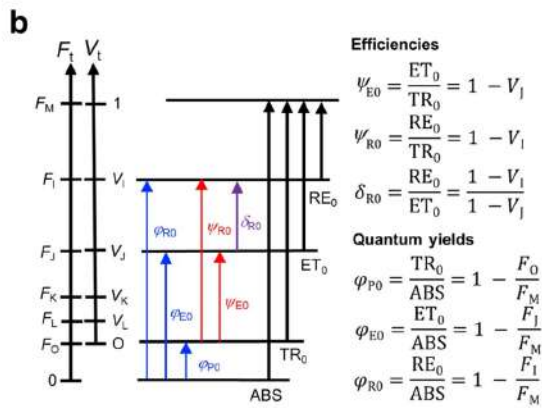
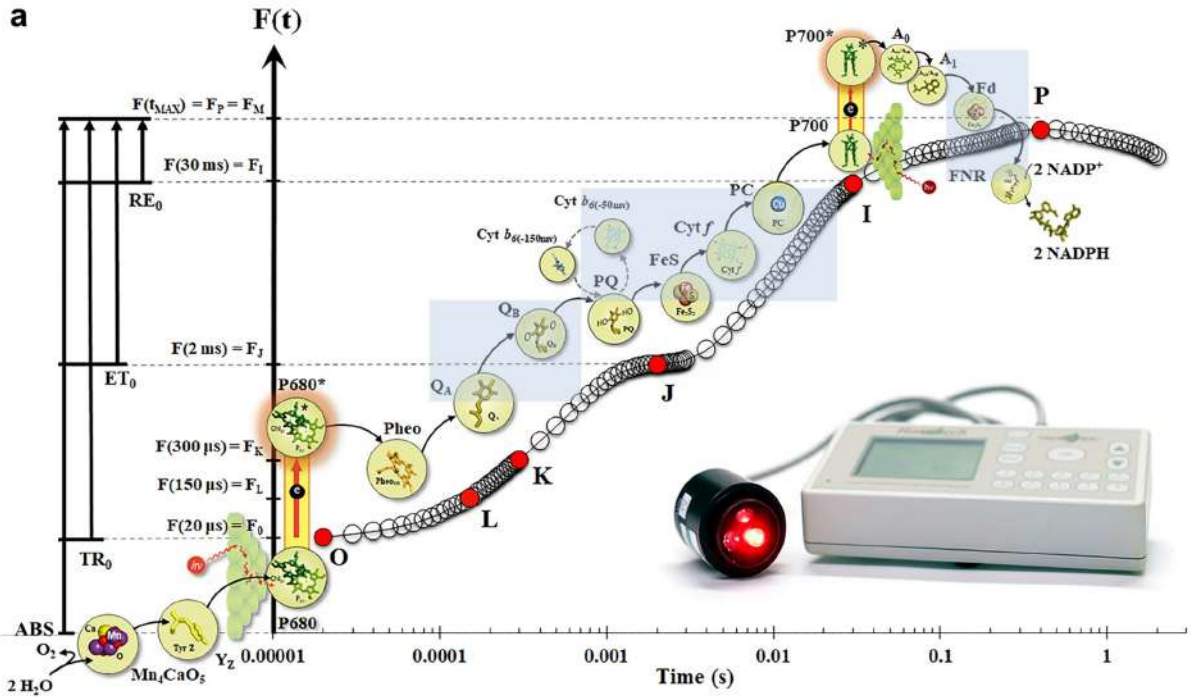


Figure S9. Chlorophyll (Chl) *a* fluorescence transient curves and important JIP-test parameters (for full form of all abbreviations used here, see Table S4). a, A possible relationship between chl *a* fluorescence transient curve and the photosynthetic electron transport. O, J, I, P are the starting points of the different phases, where “O” is for the minimal, P for the peak (maximal), J and I are for intermediate inflections. The electron transport chain, shown here, was modified from ref 26; b, Key fluorescence parameters and the definition of quantum yields, efficiencies and probabilities; c, Chl *a* fluorescence kinetic curves doubly normalized with F_O and F_M , plotted as V_i on a logarithmic time scale, for *Microcystis* FACHB-905 treated with different concentrations of AA for 41 h and the control; d-e, The radar plots for the key JIP parameters of FACHB-905 treated with different concentrations of AA for 41 h or treated with 10 mg L⁻¹ of AA for 6 h and 24 h. The areas with light blue shadows indicate the sections of the photosynthetic electron transport chain affected by AA.

Photosynthetic Oxygen Evolution
(without addition of other inhibitor/electron donor/electron acceptor)

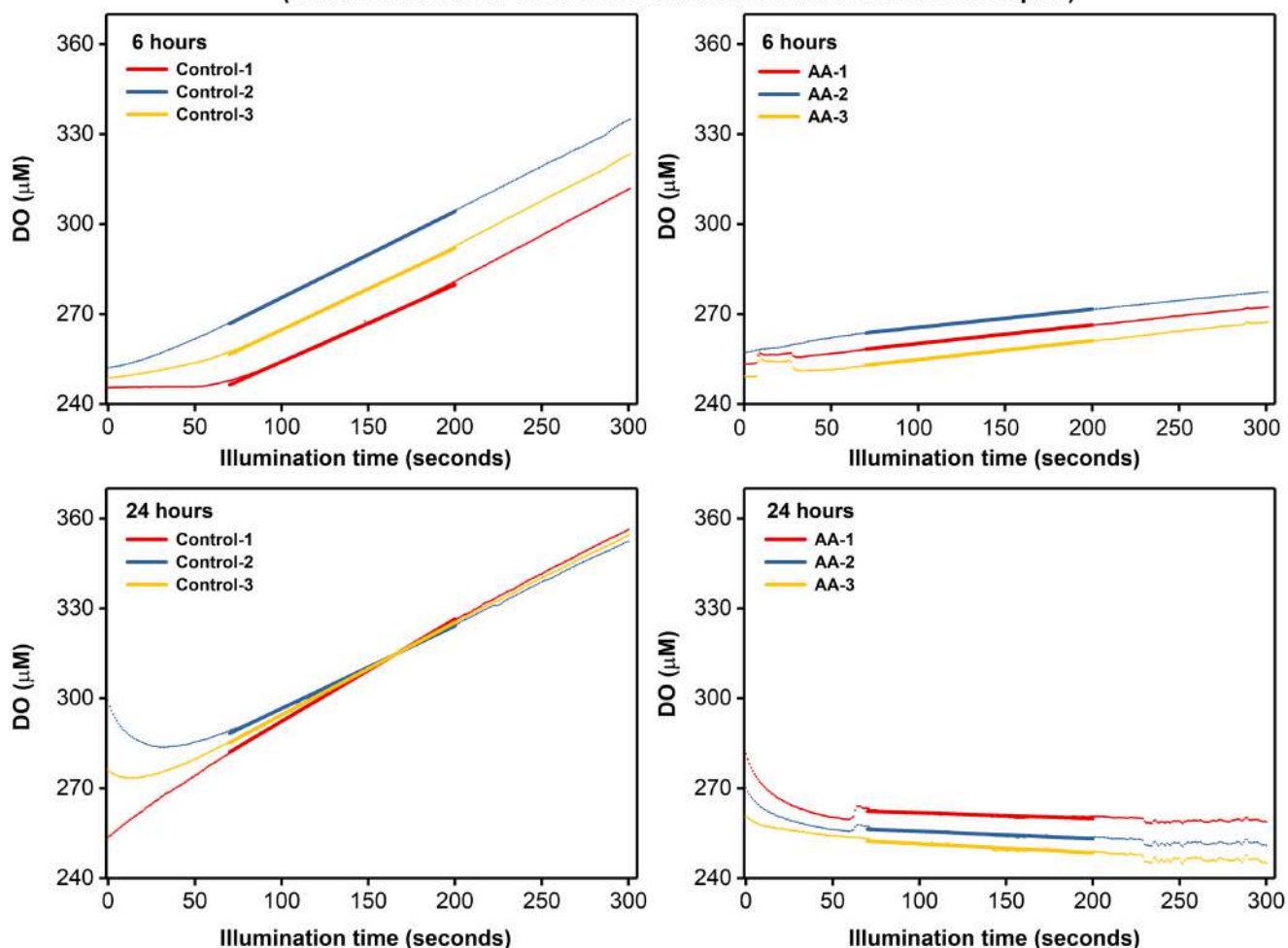


Figure S10. The photosynthetic oxygen evolution under conditions for gross photosynthesis determination (exposed to illumination without addition of any other inhibitor/electron donor/electron acceptor). The sections of dissolved oxygen (DO) vs illumination time curves with thicker lines were selected for linear fitting. The slope of the linear fitting was further divided by the concentration of Chl *a* to obtain the data shown in Table S6. The other data in Table S6 were processed using the same approach.

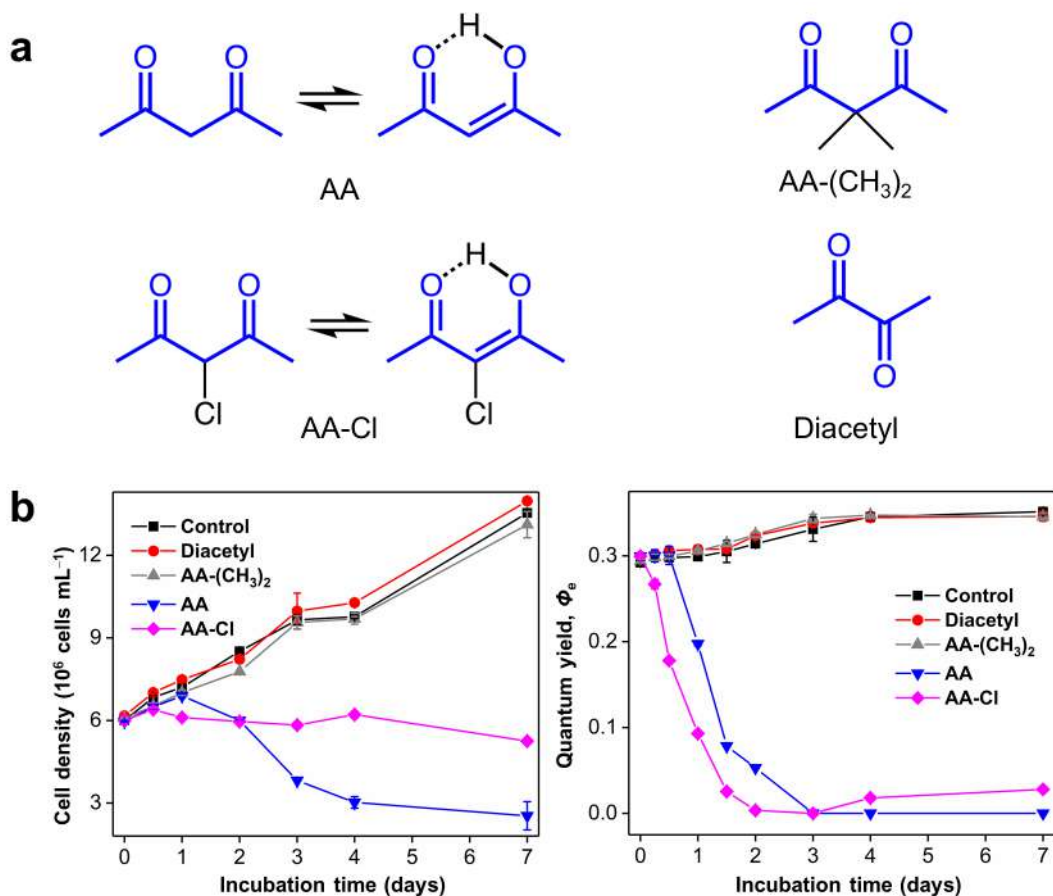


Figure S11. The molecular structures of four diketones and their cyanocidal effects on FACHB-905. a, The structure of acetylacetone (AA), AA-Cl (where one of the H atoms at the central carbon of AA were replaced with chlorine), AA-(CH₃)₂ (where both the H atoms at the central carbon were replaced with methyl groups) and diacetyl. AA and AA-Cl have enol structures due to the keto-enol tautomerization; b, The effects of the four diketones on the growth of FACHB-905 in terms of cell density and effective quantum yield (Φ_e).

REFERENCES

- (1) Roth, B. L.; Poot, M.; Yue, S. T.; Millard, P. J. Bacterial viability and antibiotic susceptibility testing with SYTOX green nucleic acid stain. *Appl. Environ. Microbiol.* **1997**, 63, 2421–2431.
- (2) Vermes, I.; Haanen, C.; Steffens-Nakken, H.; Reutellingsperger, C. A novel assay for apoptosis flow cytometric detection of phosphatidylserine expression on early apoptotic cells using fluorescein labelled annexin V. *J. Immunol. Methods* **1995**, 184, 39–51.
- (3) Wang, X. M.; Wang, X.; Wei, Z. B.; Zhang, S. J. Potent removal of cyanobacteria with controlled release of toxic secondary metabolites by a titanium xerogel coagulant. *Water Res.* **2018**, 128, 341–349.
- (4) Nikolic, M. R.; Minic, S.; Macvanin, M.; Stanic-Vucinic, D.; Velickovic, T. C. Analytical protocols in phycobiliproteins analysis. In *Pigments from Microalgae Handbook*, Springer: 2020; pp 179–201.
- (5) Sartory, D. P.; Grobbelaar, J. U. Extraction of chlorophyll a from freshwater phytoplankton for spectrophotometric analysis. *Hydrobiologia* **1984**, 114, 177–187.
- (6) Cathcart, R.; Schwiens, E.; Ames, B. N. Detection of picomole levels of hydroperoxides using a fluorescent dichlorofluorescein assay. *Anal. Biochem.* **1983**, 134, 111–116.
- (7) Winterbourn, C. C.; Hawkins, R. E.; Brian, M.; Carrell, R. The estimation of red cell superoxide dismutase activity. *Transl. Res.* **1975**, 85, 337–341.
- (8) Maehly, A.; Chance, B. Catalases and peroxidases. *Methods Biochem. Anal.* **1954**, 1, 357–424.
- (9) Placer, Z. A.; Cushman, L. L.; Johnson, B. C. Estimation of product of lipid peroxidation (malonyl dialdehyde) in biochemical systems. *Anal. Biochem.* **1966**, 16, 359–364.
- (10) Hafeman, D.; Sunde, R.; Hoekstra, W. Effect of dietary selenium on erythrocyte and liver glutathione peroxidase in the rat. *J. Nutr.* **1974**, 104, 580–587.
- (11) Ralph, P. J.; Gademann, R. Rapid light curves: a powerful tool to assess photosynthetic activity. *Aquat. Bot.* **2005**, 82, 222–237.
- (12) Platt, T.; Gallegos, C. L. Modelling primary production. In *Primary Productivity in the Sea*, Springer: 1980; pp 339–362.
- (13) Strasser, R. J.; Tsimilli-Michael, M.; Srivastava, A. *Analysis of the Chlorophyll a Fluorescence Transient*. In: Papageorgiou, G.C. and Govindjee (Eds.) *Chlorophyll a Fluorescence: A Signature of Photosynthesis*, pp 321–362, Springer: 2004.

- (14) Govindjee; Shevela, D. Adventures with cyanobacteria: a personal perspective. *Front. Plant Sci.* **2011**, 2, 28.
- (15) Stirbet, A.; Govindjee. On the relation between the Kautsky effect (chlorophyll a fluorescence induction) and Photosystem II: Basics and applications of the OJIP fluorescence transient. *J. Photochem. Photobiol. B: Biol.* **2011**, 104, 236–257.
- (16) Fiehn, O.; Kopka, J.; Dörmann, P.; Altmann, T.; Trethewey, R. N.; Willmitzer, L. Metabolite profiling for plant functional genomics. *Nat. Biotechnol.* **2000**, 18, 1157–1161.
- (17) Thompson, A.; Schäfer, J.; Kuhn, K.; Kienle, S.; Schwarz, J.; Schmidt, G.; Neumann, T.; Hamon, C. Tandem mass tags: a novel quantification strategy for comparative analysis of complex protein mixtures by MS/MS. *Anal. Chem.* **2003**, 75, 1895–1904.
- (18) Levin, Y. The role of statistical power analysis in quantitative proteomics. *Proteomics* **2011**, 11, 2565–2567.
- (19) Zhu, X.; Dao, G.; Tao, Y.; Zhan, X.; Hu, H. A review on control of harmful algal blooms by plant-derived allelochemicals. *J. Hazard. Mater.* **2021**, 401, 123403.
- (20) Li, B.; Yin, Y.; Kang, L.; Feng, L.; Liu, Y.; Du, Z.; Tian, Y.; Zhang, L. A review: Application of allelochemicals in water ecological restoration-algal inhibition. *Chemosphere* **2021**, 267, 128869.
- (21) Chaïb, S.; Pistevos, J. C. A.; Bertrand, C.; Bonnard, I., Allelopathy and allelochemicals from microalgae: An innovative source for bio-herbicidal compounds and biocontrol research. *Algal Res.* **2021**, 54, 102213.
- (22) Matthijs, H. C. P.; Jančula, D.; Visser, P. M.; Maršálek, B. Existing and emerging cyanocidal compounds: new perspectives for cyanobacterial bloom mitigation. *Aquat. Ecol.* **2016**, 50, 443–460.
- (23) Kalaji, H. M.; Jajoo, A.; Oukarroum, A.; Brestic, M.; Zivcak, M.; Samborska, I. A.; Cetner, M. D.; Łukasik, I.; Goltsev, V.; Ladle, R. J. Chlorophyll *a* fluorescence as a tool to monitor physiological status of plants under abiotic stress conditions. *Acta. Physiol. Plant.* **2016**, 38, 102–113.
- (24) Chen, Z.; Juneau, P.; Qiu, B. S. Effects of three pesticides on the growth, photosynthesis and photoinhibition of the edible cyanobacterium Ge-Xian-Mi (*Nostoc*). *Aquat. Toxicol.* **2007**, 81, 256–265.
- (25) Zhu, J.Y.; Liu, B.Y.; Wang, J.; Gao, Y.N.; Wu, Z.B. Study on the mechanism of allelopathic influence on cyanobacteria and chlorophytes by submerged macrophyte (*Myriophyllum spicatum*) and its secretion. *Aquat. Toxicol.* **2010**, 98, 196–203.
- (26) Govindjee; Shevela, D.; Bjorn, L. O. Evolution of the Z-scheme of photosynthesis: a perspective. *Photosynth. Res.* **2017**, 133, 5–15.